VIBRATIONAL RAMAN SPECTRA OF HYDROGEN DEUTERIDE IN THE CRITICAL REGION

PIOTR STANIASZEK

VIBRATIONAL RAMAN SPECTRA OF HYDROGEN DEUTERIDE IN THE CRITICAL REGION

by

Piotr Staniaszek, M.Sc. (University of Warsaw)

A Thesis submitted in partial fulfillment
of the requirements for the degree of
Master of Science

Department of Physics
Memorial University of Newfoundland

March 1987

St. John's Newfoundland

ISBN 0-315-36992-2

ABSTRACT

Lineshape data have been obtained for the polarized Raman (Q branch) spectrum of HD in the critical region (T_C = 35.91 K). The temperature dependence of the spectrum was investigated in the single phase region along isochores corresponding to the critical density (ρ_C), $0.5\rho_C$, and $2.25\rho_C$. Spectra of the liquid and vapor were also obtained along the coexistence line down to minimum temperatures of 18.14 K and 31.96 K, respectively. Emphasis is placed on the pronounced variations in lineshape observed on the critical isochore where the behaviour is interpreted in terms of three effects: (i) normal pressure broadening (ii) direct, or pure, vibrational dephasing, and (iii) a specific kind of critical broadening which occurs in the immediate vicinity of the critical point.

ACKNOWLEDGEMENTS

I wish to thank Dr. M.J. Clouter for his helpful discussions, and for considerable help in my laboratory work. Also I want to express my sense of gratitude to Dr. C.G. Deacon for his valuable help at every stage of this work. Remarks made by Dr. H. Kiefte, Dr. J. Tuszynski, Dr. J.B. Whitehead and Dr. B. Mroz helped me very much in preparing this manuscript.

My stay in St. John's during the present work would be impossible without support by a Fellowship and a Teaching Assistantship from Memorial University of Newfoundland which I gratefully acknowledge.

I am highly indebted to my wife Jadwiga, who joined me from Poland and is now with me in foggy, rainy and snowy St. John's. Thanks a million Wisia!!.

TABLE OF CONTENTS

LIST OF FIGURES

moment σ (in amagat units) versus ϵ on the critical isochores of N_2 (Ref. 20), H_2 (Ref. 25), and HD.

CHAPTER I

INTRODUCTION

Molecular hydrogen and its isotopic variations have always played a very important role in molecular physics, because they are well suited for both theoretical calculations and experimental observations. When compared to H_2 and D_2, the molecule HD has additional properties which make it unique. It is a fermion, while D_2 and H_2 are bosons. It has no center of symmetry, which results in a permanent (although small) dipole moment, and additional angle-dependent intermolecular forces not found in H_2 and D_2. Its lack of ortho and para species and larger cross section for inelastic rotational collisions[1,2] together have the result that observation of the particular phenomenon of Q-branch narrowing[3] is far more accessible than for H_2 or D_2. By comparison with H_2 and D_2, there are relatively few publications on the Raman spectra of HD.

In 1931, H.C. Urey, F.G. Brickwedde, and G.M. Murphy[4] discovered the heavy hydrogen isotopes HD and D_2, properties of which were summarized in 1932 by A. Farkas[5]. The first measurements of the Raman lineshape of liquid and solid HD were performed in 1962 by Bhatnagar and coworkers[6]. In 1972 Dion and May [3] measured Raman spectra of gaseous HD for different densities. In 1976 similar measurements were made by Witkowicz and May[7]. They published data for gaseous HD at different pressures, at room temperature and 85° K. Work by Bonamy and coworkers[8] contains theoretical considerations about lineshift and

bandwidth. This work is based on previous experimental data, and develops the concept of motional narrowing, which was introduced by Fiutak and Van Kranendonk[9] and Alekseyev, Sobelman and their coworkers[10]. Work by Marsault-Herail and coworkers[11] contains new data for rotation and rotation-vibration Raman spectra of HD compressed by argon at room temperature and 175 K. Some theoretical considerations were discussed.

There are several publications concerning the infrared spectra of HD (see Ref. 12, and 13, and references cited therein). However, this work is not directly relevant to the present experiments.

The present thesis contains Raman line-shape data of gaseous HD for the critical density(ρ_C = 357 amagat*), and for densities $2.25\rho_C$ = 803 amagat, and $0.504\rho_C$ = 180 amagat. Liquid and vapor spectra were also obtained at various temperatures from the triple point (16.6 K) through the critical point (35.91 K) to 55 K.

These experiments are a continuation of previous, lineshape studies in the vicinity of the liquid-vapor critical points which were performed in this laboratory. Since 1977 Clouter, Kiefte and coworkers[15,16] investigated the vibrational Raman spectra of N_2 and O_2 along the co-existence curve from the triple point, through the normal boiling point, to the critical point. Then similar investigations[17,18] were performed for CO, CH_4, CF_4, and for CO_2. New work about the

*The term amagat denotes the dimensionless relative density ρ/ρ_{STP} where ρ_{STP} = 0.04465 mole l^{-1} from Ref. 14.

vibrational Raman spectra of N_2 in the critical region[19,20] contains high-resolution data, recorded under isochoric conditions at densities ranging from .6 to 2 times the critical density. Related work by Tuszynski and coworkers[21,22] is strictly theoretical and develops the Landau theory of phase transitions[23] for the case of finite systems in the vicinity of the critical point. The most recent, unpublished work[24,25] is concerned with the spectra of D_2 and H_2.

Before presenting the new results for HD it is appropriate to review some background information pertaining to the theory of Raman scattering (Chap. II), and theoretical approaches to the behaviour of substances in the vicinity of the critical point (Chap. III).

CHAPTER II

THE RAMAN EFFECT

1. HISTORICAL REVIEW

In 1921 Prof. C.V. Raman began a series of experimental studies on the scattering of light by transparent media. These investigations revealed the presence of a feeble type of secondary radiation of altered wavelength in liquids, crystals and glasses. The intensity of the secondary radiation was found to be dependent on the wavelength of the incident radiation and it was strongly polarized. It was recognized immediately by Raman as a new phenomenon of a fundamental character scattering, analogous to the Compton effect. The first announcment of the discovery of this phenomenon was made on March 16, 1928[26]. The possibility of the occurrence of this process had been predicted by A. Smekal in 1923[27]. Smekal pointed out that scattering might be accompanied by a change in the energy of the scattering system, with the scattered radiation differing from the incident radiation by the frequencies characteristic of the system. This idea was further developed by Kramers and Heisenberg[28] in their treatment of the quantum theory of dispersion, and also by Dirac[29] in his radiation theory.

After announcment of Raman's discovery, investigations were carried out by many workers around the world. During the twelve years after this event, the number of papers published on various aspects of the phenomenon was more than

1800. In the early stages, the interest changed from an explanation of the Raman effect, to the correlation of the effect with the modes of molecular vibration. During this period (1928-1940), more than 2500 different substances were investigated. Later, considerable progress was made in knowledge of the Raman spectra of crystals and their interpretations.

Since about 1965 the laser was has been used extensively in the study of the Raman effect. Laser light is monochromatic, has small bandwidth (in the present experiment 10 GHz), and may be highly intense and polarized. For these reasons investigations of the Raman effect using lasers are much simpler, spectra are recorded easily in small amounts of samples or in gases under low pressure, and precise information can be obtained on the width and fine structure of the Raman lines. These latter advantages are most important for the investigation of the shape of the Raman spectrum in the present work.

The above section is based primarily on Ref. 30.

2. CLASSICAL THEORY OF RAMAN SCATTERING

The following classical treatment of the Raman effect, and the associated Rayleigh effect (i.e. scattering without change of frequency), is based primarily on References 31, 32 and 33.

Let us consider a molecule which vibrates and rotates in an electric field. This field oscillates with the frequency ν_o, ($\mathbf{E} = \mathbf{E}_o \sin 2\pi\nu_o t$), and the electron cloud of the molecule is deformed, in response to the applied field. This deformation gives rise to an electric dipole moment, P, which may be expressed as:

$$|\mathbf{P}| = \alpha |\mathbf{E}| = \alpha |\mathbf{E}_o| \sin 2\pi\nu_o t , \qquad (2\text{-}1)$$

where α is the molecular polarizability and is a second order tensor. The polarizability is modulated by the motions of the molecule (vibrations or rotations) and may be expressed as:

$$\alpha = \alpha_o + \alpha_1 \sin 2\pi\nu_m t , \qquad (2\text{-}2)$$

where ν_m is a given normal mode of vibration or rotation.

By subsituting Eq. (2-2) into Eq. (2-1) the general expression for the dipole moment is obtained in the form[33]:

$$P = \alpha_o E_o \sin 2\pi\nu_o t + \frac{1}{2}\alpha_1 E_o [\cos 2\pi(\nu_o - \nu_m)t - \cos 2\pi(\nu_o + \nu_m)t] \qquad (2\text{-}3)$$

We may note that the interaction between the molecule and the incident radiation gives not only radiation with the same frequency ν_o (Rayleigh scattering), but radiations which have frequencies $(\nu_o - \nu_m)$ and $(\nu_o + \nu_m)$. The Raman lines shifted toward longer wavelength $(\nu_o - \nu_m)$ are called Stokes lines and those

displaced toward shorter wavelength ($\nu_o + \nu_m$) are called anti-Stokes lines.

The polarizability tensor α may be decomposed into a sum of two terms[31]:

$$\begin{bmatrix} \alpha_{xx} & \alpha_{xy} & \alpha_{xz} \\ \alpha_{yx} & \alpha_{yy} & \alpha_{yz} \\ \alpha_{zx} & \alpha_{zy} & \alpha_{zz} \end{bmatrix} = \frac{1}{3}\begin{bmatrix} 1 & 0 & 0 \\ 0 & 1 & 0 \\ 0 & 0 & 1 \end{bmatrix}\bar{\alpha} + \begin{bmatrix} \alpha_{xx}-\frac{1}{3}\bar{\alpha} & \alpha_{xy} & \alpha_{xz} \\ \alpha_{yx} & \alpha_{yy}-\frac{1}{3}\bar{\alpha} & \alpha_{yz} \\ \alpha_{zx} & \alpha_{zy} & \alpha_{zz}-\frac{1}{3}\bar{\alpha} \end{bmatrix} \qquad (2\text{-}4)$$

and

$$\alpha \equiv \frac{1}{3}\bar{\alpha}\mathbf{I} + \beta \ , \qquad (2\text{-}4a)$$

where $\mathbf{I}$ is the unit tensor and $\bar{\alpha} = \mathrm{Tr}(\alpha_{ij}) = \alpha_{xx} + \alpha_{yy} + \alpha_{zz}$. The diagonal tensor $\bar{\alpha}\mathbf{I}$ is independent of the orientation of the molecule with respect to a fixed referenee frame, because the diagonal tensor element α_{ii} is a coordinate-independent, scalar quantity. Thus we may split the polarizability tensor (scattering correlation function) into an angle-independent part $\bar{\alpha}\mathbf{I}$ and an angle-dependent part β, each of which may be investigated experimentally[32] (Fig. 1).

In the case (a) the source of radiation is polarized (laser light) and in the case (b) the source of light gives unpolarized radiation (for example mercury arc). The scattered light, at 90^0 along the y-axis for example, may be analyzed for polarization parallel to the z axis (intensity I_z) and polarization parallel to the x axis (I_x). The ratio:

$$\rho = \frac{I_z}{I_x} \ , \qquad (2\text{-}5)$$

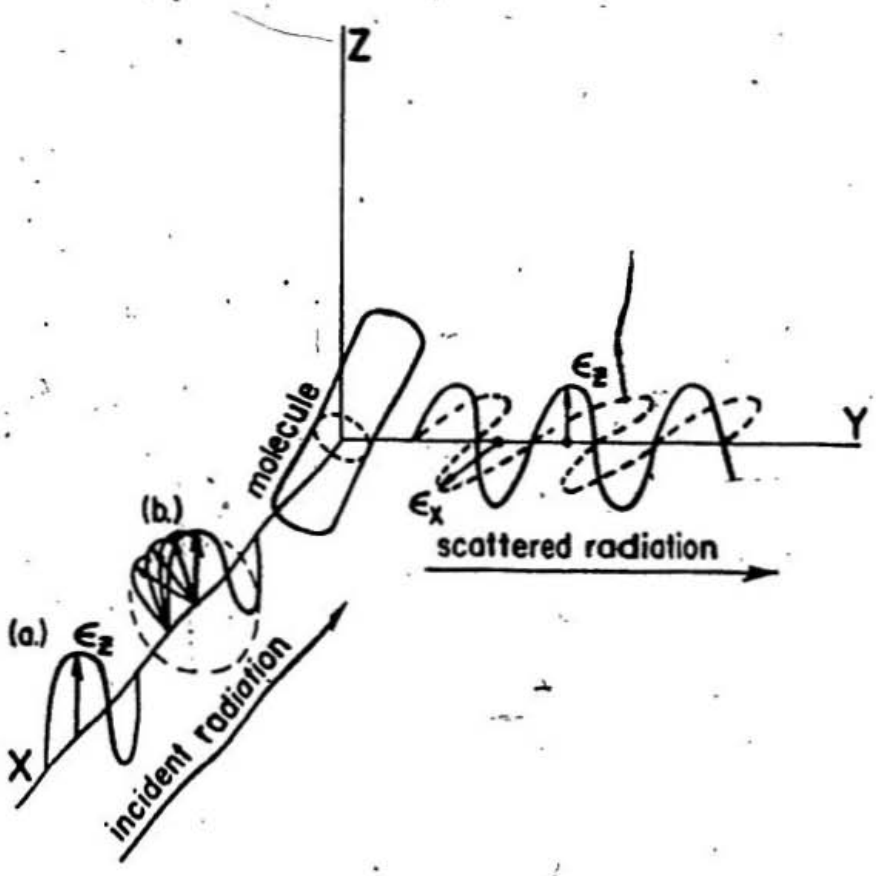

FIG. 1. The light scattered by an asymmetric molecule is unpolarized, without regard to polarization state of incident radiation: (a) polarized (for example laser light) (b) unpolarized (for example mercury arc). ϵ_z, and ϵ_x are polarizability vectors explained in the text (in the next section).

when incident light is polarized along the z axis (case (a)), is expressed as:

$$\rho_p = \frac{I_{zz}}{I_{zz}} = \frac{3\gamma^2}{45\bar{\alpha}^2+4\gamma^2} , \tag{2-6}$$

$$\gamma^2 = \frac{1}{2}[(\alpha_{zz}-\alpha_{yy})^2+(\alpha_{yy}-\alpha_{zz})^2+(\alpha_{zz}-\alpha_{zz})^2+6(\alpha_{xy}^2+\alpha_{yz}^2+\alpha_{zz}^2)] , \tag{2-6a}$$

for case (b), when incident light is unpolarized, then:

$$\rho_u = \frac{6\gamma^2}{45\bar{\alpha}^2+7\gamma^2} . \tag{2-7}$$

By measuring I_{zz} and I_{zz} we may draw some conclusions about the polarizability tensor and about the symmetry properties of molecule. For example, if $\alpha_{zz} = \alpha_{yy} = \alpha_{zz}$, then $\rho_p = 0 = \rho_u$. If $\alpha_{zz} = \alpha_{yy} \neq \alpha_{zz}$, then by measuring ρ_p and ρ_u we may determine α_{zz} and α_{zz}. For this kind of experiment we may define isotropic and anisotropic intensities:

$$I_{isotropic} = I_{zz} - \frac{4}{3} I_{zz} = \frac{1}{9}(Tr\,\alpha)^2 = \bar{\alpha}^2. \tag{2-8}$$

$$I_{anisotropic} = I_{zz} \approx \gamma^2. \tag{2-9}$$

The first one is obviously independent of the molecular orientation. The intensity I_{zz} is called anisotropic because it depends on the off-diagonal terms of the tensor α, (i.e. of the tensor β) and is dependent on the molecular orientation (i.e. on molecular rotations). The present work is restricted to the study of vibrational Raman spectra where the isotropic intensity is most important. To consider more closely this intensity it is necessary to apply the quantum mechanical theory of the Raman effect.

3. QUANTUM THEORY OF THE RAMAN EFFECT

The classical Hamiltonian for a system of N nonrelativistic particles, and for the electromagnetic field generated by them, has the form[34,35,36]:

$$H = K + V_c + H_{rad}, \tag{3-1}$$

where K is kinetic energy,

$$K = \sum_{j=1}^{N} \frac{1}{2}\left[\mathbf{p}_j - \frac{e_j \mathbf{A}_j(\mathbf{x}_j)}{c}\right]^2, \tag{3-2}$$

V_c is Coulomb interaction:

$$V_c = \sum_{i>j} \frac{e_i e_j}{4\pi(\mathbf{x}_i - \mathbf{x}_j)}, \tag{3-3}$$

and H_{rad} is free field Hamiltonian:

$$H_{rad} = \frac{1}{2}\int_V dV(|\mathbf{B}|^2 + |\mathbf{E}|^2) = \frac{1}{2}\int_V dV\left[|\nabla\times\mathbf{A}|^2 + \left|\frac{1}{c}\frac{\partial \mathbf{A}}{\partial t}\right|^2\right]. \tag{3-4}$$

In these equations $\mathbf{A}$ is the vector potential of the magnetic field, $\mathbf{p}_j$ is the momentum vector of j-th particle.

The vector potential may be chosen in such a way that it satisfies the Coulomb gauge, and from the Maxwell equations it is easy to obtain[35] the wave equation for $\mathbf{A}$

$$\nabla^2\mathbf{A} - \frac{1}{c^2}\frac{\partial^2 \mathbf{A}}{\partial t^2} = 0, \tag{3-5}$$

then $\mathbf{A}$ may be expanded in a Fourier Series assuming a periodic boundary condition for A encloseed in a box taken to be a cube of side $L = V^{\frac{1}{3}}$:

$$\mathbf{A}(\mathbf{x},t) = \frac{1}{\sqrt{V}}\sum_{\mathbf{k}}\sum_{\alpha} c_{\mathbf{k},\alpha}(t)\epsilon^{(\alpha)}e^{i\mathbf{k}\cdot\mathbf{x}} + c^{*}_{\mathbf{k},\alpha}(t)\epsilon^{(\alpha)}e^{-i\mathbf{k}\cdot\mathbf{x}} \quad . \tag{3-6}$$

Here $c_{\mathbf{k},\alpha}(t) = c_{\mathbf{k},\alpha}(0)e^{-i\omega t}$, $\omega = |\mathbf{k}|c$, $\alpha = 1, 2$ and $\epsilon^{(1)}, \epsilon^{(2)}$ are called polarization vectors which depend on the propagation direction $\frac{\mathbf{k}}{|\mathbf{k}|}$ in such a way that all three form a right-handed set of mutually orthonormal vectors.

If we define generalized positions and momenta as

$$Q_{\mathbf{k},\alpha} = \frac{1}{c}(c_{\mathbf{k},\alpha} + c^{*}_{\mathbf{k},\alpha}) \quad , \tag{3-7}$$

$$P_{\mathbf{k},\alpha} = \frac{-i\omega}{c}(c_{\mathbf{k},\alpha} - c^{*}_{\mathbf{k},\alpha}) \quad , \tag{3-8}$$

then we may express

$$H_{rad} = \sum_{\mathbf{k}}\sum_{\alpha}\frac{1}{2}(P^{2}_{\mathbf{k},\alpha} + \omega^{2}Q^{2}_{\mathbf{k},\alpha}) \quad . \tag{3-9}$$

From this equation it is clear that the radiation field may be described by a system of harmonic oscillators.

The above consideration was within the framework of classical electrodynamics. According to the assumption which was made by Max Planck in 1901, each oscillator has an energy which is integral multiple of $\hbar\omega$. Following the Dirac formalism, the canonical dynamical variables of radiation oscillators are operators, not numbers. We may introduce operators $a_{\mathbf{k},\alpha}$ and $a^{+}_{\mathbf{k},\alpha}$, defined as:

$$a_{\mathbf{k},\alpha} = \frac{1}{\sqrt{2\hbar\omega}}(\omega Q_{\mathbf{k},\alpha} + iP_{\mathbf{k},\alpha}) \;\; ; \;\; c_{\mathbf{k},\alpha} = c\sqrt{\frac{\hbar}{2\omega}}a_{\mathbf{k},\alpha} \tag{3-10}$$

$$a^{+}_{\mathbf{k},\alpha} = \frac{1}{\sqrt{2\hbar\omega}}(\omega Q_{\mathbf{k},\alpha} - iP_{\mathbf{k},\alpha}) \;\; ; \;\; c^{*}_{\mathbf{k},\alpha} = c\sqrt{\frac{\hbar}{2\omega}}a^{+}_{\mathbf{k},\alpha} \tag{3-11}$$

where $a_{\mathbf{k},\alpha}$ and $a^{+}_{\mathbf{k},\alpha}$ are the annihilation and creation operators well known from quantum mechanics. Their multiplication gives a number operator

$$N_{\mathbf{k},\alpha} = a^{+}_{\mathbf{k},\alpha} a_{\mathbf{k},\alpha} \tag{3-12}$$

and we may introduce the so-called number states

$$N_{k,\alpha} \mid n_{\mathbf{k},\alpha} > = n_{\mathbf{k},\alpha} \mid n_{\mathbf{k},\alpha} > \tag{3-12a}$$

Now, Eq. (3-6) for the quantum mechanical magnetic potential has the form:

$$\mathbf{A}(\mathbf{x},t) = \frac{1}{\sqrt{V}} \sum_{\mathbf{k}} \sum_{\alpha} c \sqrt{\frac{\hbar}{2\omega}} \tag{3-13}$$

$$\times \left[a_{\mathbf{k},\alpha} \epsilon^{(\alpha)} \exp(i\,\mathbf{k}\cdot\mathbf{x} - i\omega t) + a^{+}_{\mathbf{k},\alpha}\, \epsilon^{(\alpha)} \exp(-i\,\mathbf{k}\cdot\mathbf{x} + i\omega t) \right]$$

and the Hamiltonian (3-1) may be rewritten in the form:

$$H = H_o + H_I(t) \tag{3-14}$$

where H_0 is the part of the Hamiltonian connected with the energy of particles and the energy of the pure field both of which are constant. The $\mathbf{H}_I(t)$ is the part of the Hamiltonian connected with the coupling of the field and the particles, and may be simply expressed as

$$H_I(t) = H_{Int} = \sum_{j=1}^{N} -\frac{e}{mc} A(\mathbf{x}_j, t)\mathbf{p}_j + \frac{e^2}{2mc^2} \mathbf{A}(\mathbf{x}_j, t)\mathbf{A}(\mathbf{x}_j, t) \,. \tag{3-15}$$

When we treat $\mathbf{H}_I$ as a time dependent perturbation to $\mathbf{H}_o$, we may introduce the energy eigenfunctions $\mathbf{U}_k(\mathbf{x})$ such that

$$H_o\, U_k(\mathbf{x}) = E_k\, U_k(\mathbf{x}) \tag{3-16}$$

in the absence of a time dependent perturbation.

The time-dependent Schroedinger equation is

$$(H_o + H_I)\Psi = i\hbar\frac{\partial\Psi}{\partial t} \quad , \tag{3-17}$$

where

$$\Psi = \sum_k C_k(t)U_k(\mathbf{x})\exp(-i\frac{E_k\, t}{\hbar}) \quad . \tag{3-17a}$$

From first-order perturbation theory, $C_k(t)$ is expressed

$$C_k^{(1)}(t) = \frac{1}{i\hbar}\int_0^t dt' < k \mid H_I(t') \mid l > \exp\left\{i\frac{(E_m - E_l)t'}{\hbar}\right\} \quad . \tag{3-18}$$

When we have elastic scattering of light (Rayleigh scattering, see Fig. 2a), the only nonzero contributions to the $C_k^{(1)}(t)$, are from

$$H_{int} = \sum_j \frac{e^2}{2mc^2}\mathbf{A}(\mathbf{x}_j,t)\mathbf{A}(\mathbf{x}_j,t) \approx a_{k,\alpha}a^+_{k,\alpha} + a^+_{k,\alpha}a_{k,\alpha} \quad . \tag{3-19}$$

In this case, the atom before and after light scattering is in the same state, and the number of photons is constant, i.e. $|I> = |F>$ and $| n_{k\alpha}> = | n_{k'\alpha}>$. The transition amplitude is expressed by:

$$C_k^{(1)}(t) = const \times \delta_{IF}\epsilon^{(\alpha)}\epsilon^{(\alpha')}\int_0^t \exp\left[i\frac{(E_F - E_I + \hbar(\omega' - \omega))t_2}{\hbar}\right]dt_2 \quad . \tag{3-20}$$

For the case of inelastic light scattering (Raman effect), we may consider two cases[34] (Fig. 2b, and 2c). In the first case, there is absorption of a photon $| n_{k\alpha}> \rightarrow | n_{k\alpha}-1>$, and the atom is shifted from the initial state $|I>$ to the intermediate state $|M>$, after this, there is emission of the photon, and we have the same number of photons $| n_{k\alpha}> = | n_{k'\alpha'}>$, but the wavelengths are

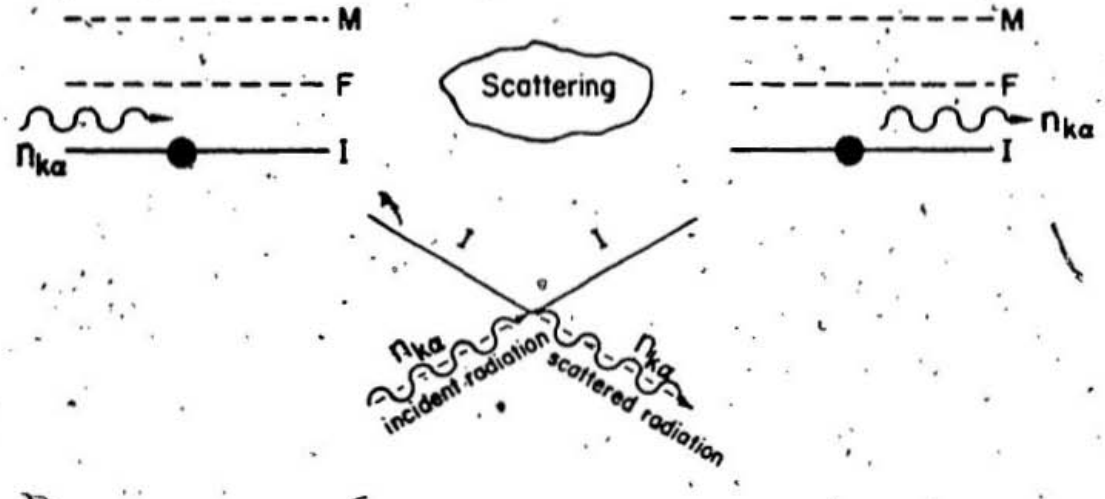

FIG. 2a. Rayleigh scattering. I-initial state of molecule, F-final state of molecule, M-intermediate state of molecule, $n_{k,\alpha}$-number of photons with wavevector **k** and polarizability along $\epsilon^{(\alpha)}$ direction.

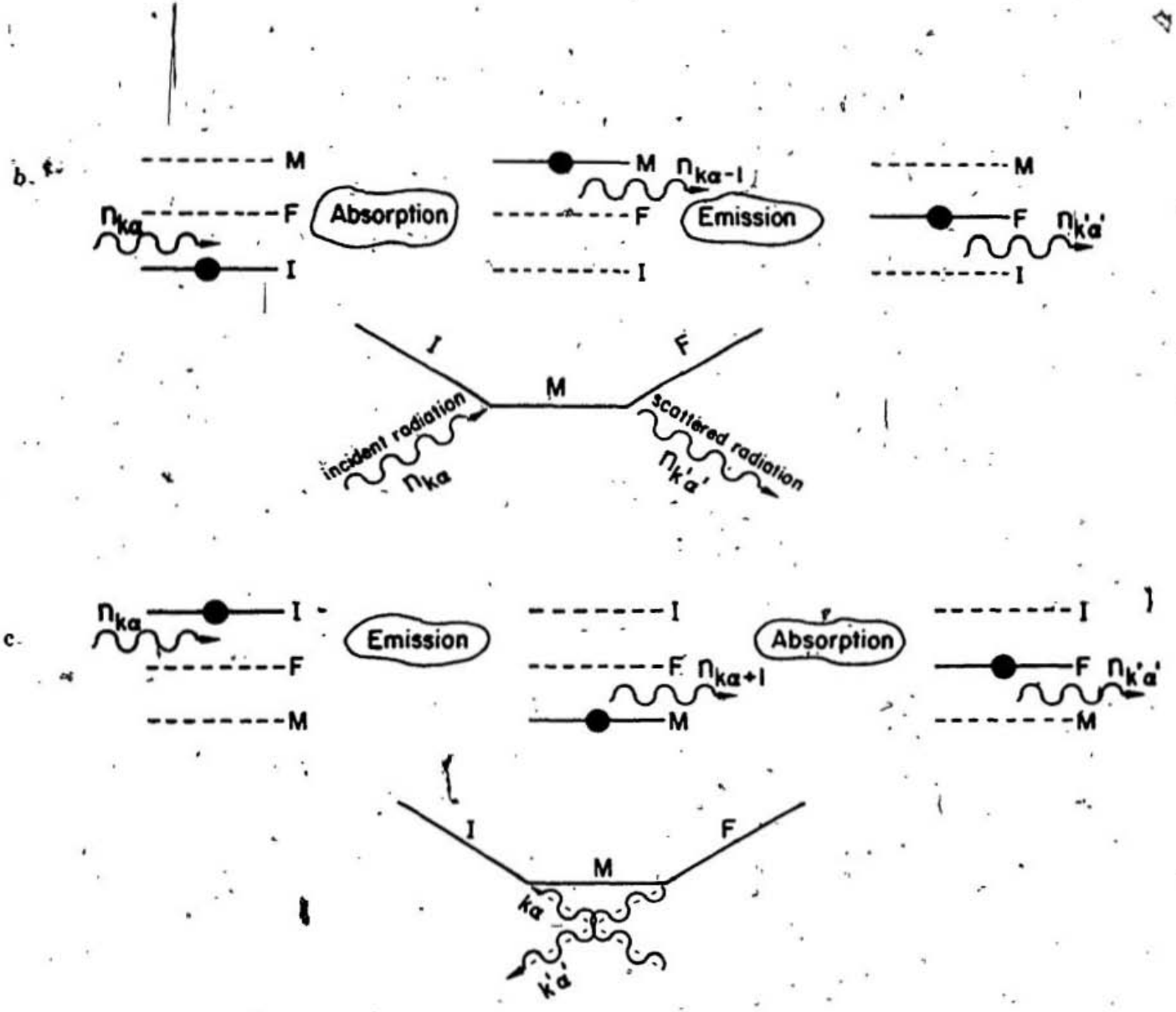

FIG. 2b. and 2c. Raman scattering. In these cases scattered radiation is polarized along the $\epsilon^{(\alpha')}$ direction and have wavevector $\mathbf{k}'$. (See explanation in the text).

different, the polarization is changed, and the atom is in the final state different from the initial one.

The second process has emission at first, and absorption after, and once again, the atom is in a different final state, the wavelength of light is shifted, and the polarization is changed[34] (see Fig. 2c). In these cases, we should use second order transition amplitudes (for simplicity we put $\hbar=1$):

$$C^{(2)}(t) = const \times (\alpha_{\alpha'\alpha})_{IF} \int_0^t dt_2 \exp[i(E_F - E_I + \omega' - \omega)t_2] \ , \qquad (3\text{-}21)$$

where:

$$(\alpha_{\alpha'\alpha})_{IF} = < I \mid \epsilon^{(\alpha)} \alpha \epsilon^{(\alpha')} \mid F > \ , \qquad (3\text{-}22)$$

and

$$(\alpha_{\alpha'\alpha})_{IF} = \sum_M \frac{< F \mid \mathbf{p}\cdot\epsilon^{(\alpha')} \mid M >< M \mid \mathbf{p}\cdot\epsilon^{(\alpha)} \mid I >}{E_M - E_I - \omega} + \qquad (3\text{-}23)$$

$$+ \frac{< F \mid \mathbf{p}\cdot\epsilon^{(\alpha)} \mid M >< M \mid \mathbf{p}\cdot\epsilon^{(\alpha')} \mid I >}{E_M - E_I + \omega}$$

Also, $\alpha_{\alpha'\alpha} = \epsilon^{(\alpha)} \alpha \epsilon^{(\alpha')}$ is the polarizability tensor, as introduced earlier in the framework of classical mechanics. Eq. (3-23) is called the Kramers-Heisenberg equation.

According to the character of the intermediate state we may consider three cases[37] (see Fig. 3):

1)Normal Raman Scattering - where the intermediate state is between two electronic states,

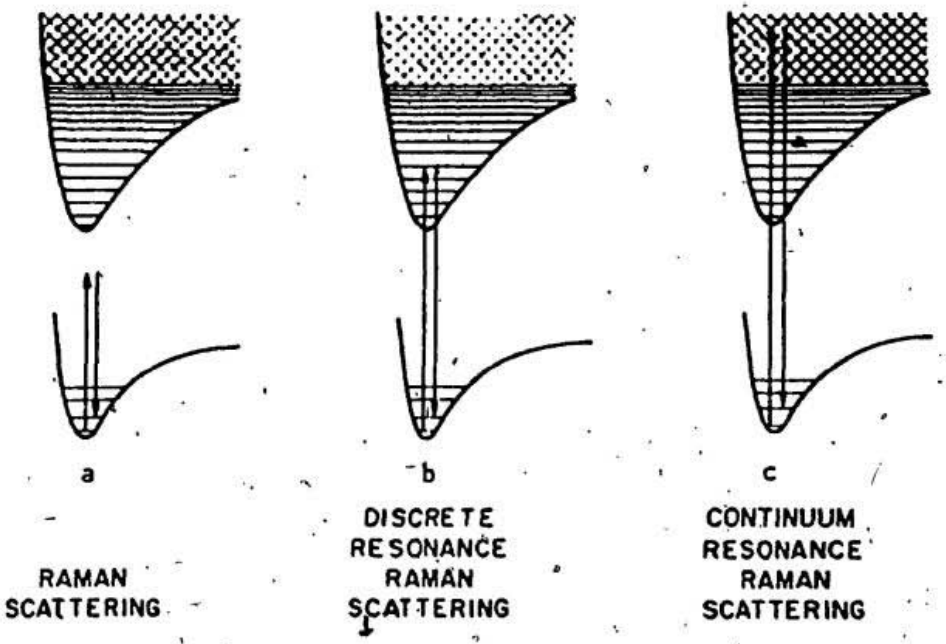

FIG. 3. Classification of Raman scattering from diatomic molecules according to the laser frequency.

(a) The incident laser frequency is far from resonance with any real electronic transition so **Normal Raman Scattering** is observed.

(b) The incident laser frequency is in the region of discrete levels of a single electronic intermediate state.

We term this process **Discrete Resonance Raman Scattering**.

(c) The incident frequency is in the range of dissociative continuum levels.

We label this process **Continuum Resonance Raman Scattering**. (From Ref. 37)

2) Discrete Resonant Raman Scattering - where the intermediate state is some discrete state of higher electronic energy,

3) Continuum Resonance Raman Scattering, where the intermediate state is within an electronic-energy continuum.

Roughly speaking the motions of the molecule may be divided into vibrational motion and rotational motion. In the first approximation we may assume that molecule is a rigid rotator which has energy[33]:

$$E_{ROT} = B_v J(J+1) \quad , \tag{3-24}$$

where B_v is rotational constant $\left(B_v = \frac{1}{8\pi^2 cI}\right)$, I is moment of inertia and J is the quantum number of the rotational state. Additionally we may suppose that this rotator vibrates as a harmonic oscillator and the energy of this vibration may be written as:

$$E_{VIB} = \nu_{osc}\left(v+\frac{1}{2}\right) \tag{3-25}$$

When we take into consideration deformation of the molecule during rotation, anharmonicity of vibrations and coupling between rotation and vibration, then the picture becomes more complicated, but the states of a molecule such as H_2 may be depicted as in Fig. 4. The frequencies for different modes of motion in a given state may be expressed as[33]:

$$\nu = \nu_e + \nu_v + \nu_r \tag{3-26}$$

where

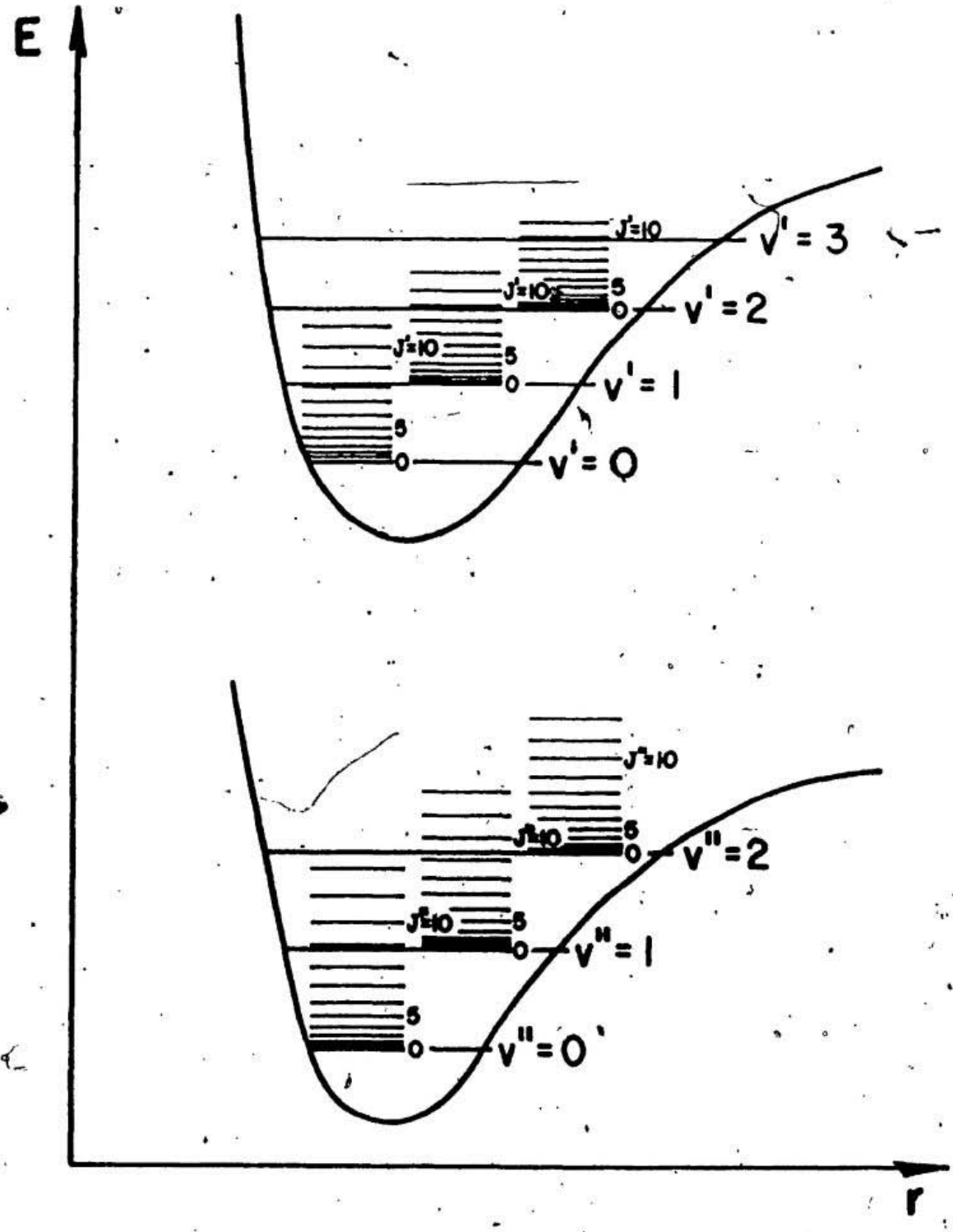

FIG. 4. Vibrational and rotational levels of two electronic states of a molecule (schematic). Only the first few rotational and vibrational levels are drawn in each case. (Ref. 33)

ν_e = frequency due to the given electronic state.

ν_v = frequency due to the vibration of molecule.

ν_r = frequency due to the rotation of molecule.

The value: $\nu_0 = \nu_e + \nu_v$ is a constant for a specific vibrational transition, but ν_r is variable and depends on the different values of the rotational quantum number in the upper and lower states. By studying the matrix elements

$$M_{Fl} = \langle F \mid \mathbf{p}\cdot\epsilon^{(\alpha')} \mid M \rangle \langle M \mid \mathbf{p}\cdot\epsilon^{(\alpha)} \mid I \rangle \ , \qquad (3\text{-}27)$$

we may infer selection rules for the Raman effect. Namely[33], for vibrational transitions:

$$\Delta v = \pm 1 \ , \qquad (3\text{-}28)$$

and for rotational transitions :

$$\Delta J = 0 \ , \pm 2 \ . \qquad (3\text{-}29)$$

For the other combinations of the states the matrix elements give zero values.

Thus for a given vibrational transition there are three branches corresponding to;

$$\Delta J = +2 \text{ and } \Delta\nu = \Delta\nu_0 + B_v'(J+2)(J+3) - B_v''J(J+1) \ , \qquad (3\text{-}30a)$$

which is called the S - branch;

$$\Delta J = 0 \text{ and } \Delta\nu = \Delta\nu_0 + (B_v' - B_v'')J(J+1) \ , \qquad (3\text{-}30b)$$

which is called the Q - branch;

$$\Delta J = -2 \text{ and } \Delta\nu = \Delta\nu_0 + B_v'J(J-1) - B_v''J(J+1) \ , \qquad (3\text{-}30c)$$

which is called the O - branch. Generally $B_{v'} \approx B_{v''}$, such that $\Delta\nu = \Delta\nu_e$, and for this reason the Q branch transitions are referred to as pure vibrational transitions. This thesis is concerned exclusively with the Q branch of HD.

Besides the selection rules, the Franck-Condon Principle also governs the transition probabilities. The basic idea[33] is indicated in Fig. 5. The transitions vertically upward or downward in the potential energy diagram are most intense if the overlap integral:

$$R \approx \int dr\, \Psi_{v'} \Psi_{v''} \tag{3-31}$$

is maximum (here $\Psi_{v'}$, $\Psi_{v''}$ are wavefunctions corresponding to the vibrational levels v' and v'').

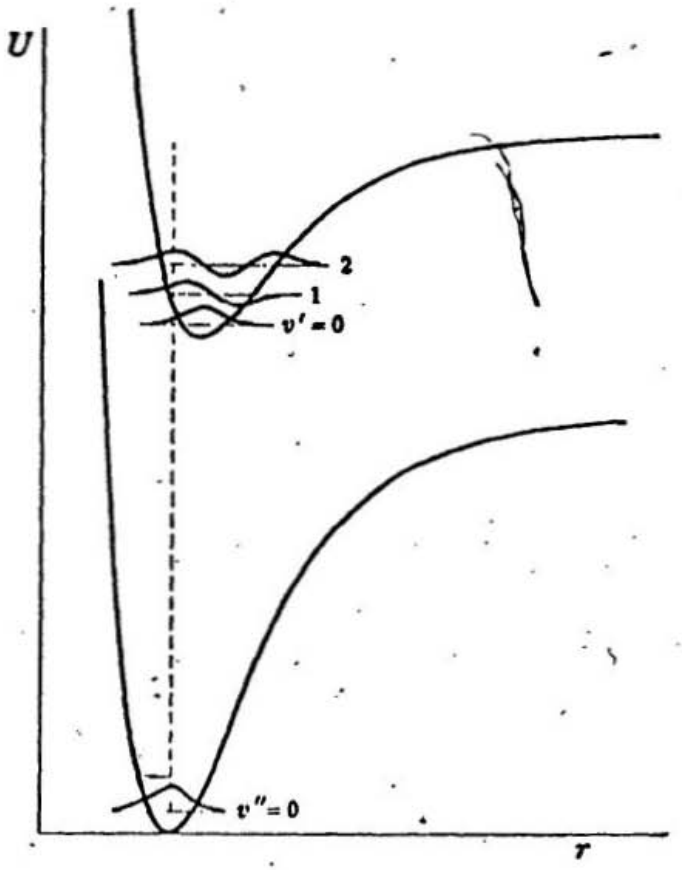

FIG. 5. Franck-Condon principle according to wave mechanics. The potential curves are so drawn that the "best" overlapping of the eigenfunctions occurs for $v' = 2$, $v'' = 0$ (see the broken vertical line). (Ref. 32)

4. SPECTRAL LINE SHAPE STUDIES, AND INTERMOLECULAR INTERACTIONS

The expression for the differential cross-section for Raman scattering into a solid angle $d\Omega$ and frequency range $[\omega, \omega + d\omega]$ was derived in 1931 by Placzek[38], and is proportional to the polarizability tensor:

$$\frac{d^2\sigma}{d\Omega d\omega} = \left(\frac{2\pi}{\lambda}\right)^2 \sum_{I,F} | <I \mid \epsilon^{(\alpha)} \alpha \epsilon^{(\alpha')} \mid F> |^2 \rho_I \ \delta(E_I - E_P + \omega) \qquad (4\text{-}1)$$

where λ is the wavelength of scattered light, ρ_I is the probability that the system is initially in state $|I>$, $\epsilon^{(\alpha)}$ and $\epsilon^{(\alpha')}$ are polarization vectors introduced earlier, and δ is the Dirac delta function.

The scattering intensity is proportional to the cross-section and we may write it using the Fourier transform of the Dirac delta[39] function

$$I(\omega) \approx \sum_{IF} \int_{-\infty}^{+\infty} dt \exp(i(\omega - E_F + E_I)t) \mid <I \mid \epsilon^{(\alpha)} \alpha \epsilon^{(\alpha')} \mid F> |^2 \rho_I \ . \qquad (4\text{-}2)$$

From quantum mechanics[31]

$$\sum_F <I \mid A \mid F><F \mid B \mid I> = <I \mid A \cdot B \mid I> \qquad (4\text{-}2a)$$

$$\sum_I \rho_I <I \mid A \cdot B \mid I> = <A \cdot B> \qquad (4\text{-}2b)$$

$$\alpha(t) = e^{iHt} \alpha e^{-iHt} \qquad (4\text{-}2c)$$

where $<C>$ is the equilibrium ensemble average of the operator inside the bracket.

Finally we obtain:

$$I(\omega) \approx \int_{-\infty}^{+\infty} dt e^{i\omega t} <\alpha_{\alpha\alpha'}(t)\alpha_{\alpha\alpha'}(0)> \qquad (4\text{-}3)$$

or:

$$C(t) \equiv <\alpha_{\alpha\alpha'}(t)\alpha_{\alpha\alpha'}(0)> = \int_{-\infty}^{+\infty} d\omega e^{-i\omega t} I(\omega) \qquad (4\text{-}3a)$$

Then the spectral density of a band contour and the correlation function of α are mutual Fourier transforms[31]. The C(t) is an average scalar product of the observed polarization tensor taken at two different times. The $\alpha_{\alpha\alpha'}(t)$ is fixed in the molecule or within a molecular group. Variations of molecular positions and orientations as well as variations of vibrational amplitudes and phase relations determine the time dependence of C(t). Because we only observe averages, then we must take the average value, and C(t) is a statistical quantity[31].

We may expand $\alpha(t)$ into a series in terms of the atomic displacement coordinates (normal coordinates) of the vibrational mode, j:

$$\alpha(t) = \alpha_e(t) + \sum_j \frac{\partial \alpha(t)}{\partial Q_j(t)} \Big|_{Q_j(t)=0} Q_j(t) + \cdots \qquad (4\text{-}4)$$

$$I_{isotropic} \approx \int_{-\infty}^{+\infty} dt e^{i\omega t} \sum_j <Q_j^A(t) Q_j^B(0)> \cdot <\sum_j \frac{\partial \alpha^A}{\partial Q_j} \frac{\partial \alpha^B}{\partial Q_j}> \qquad (4\text{-}5)$$

The first part of Eq. (4-5) is associated with the vibrational motion of molecule, the second with rotational. $<Q_j^A(t)\, Q_j^B(0)>$ is the correlation function between vibrational modes of the particle of interest (B) and the neighbouring particles,

(including the particle of interest). The influence of the neighbouring particles on the particle of interest is reflected by processes, which are observed as broadening of the spectral profile. These processes are called Vibrational Relaxation Processes and they may be divided into five groups[31,40] (see Fig. 6):

(a) Vibrational Energy Relaxation.

Some authors call this process Population Relaxation, or by analogy to nuclear-magnetic relaxation - T_1 process. In this process molecules, which are in excited vibrational levels return to the ground level and dissipate the energy difference into the translational energy of surrounding molecules.

(b) Resonance Vibrational Energy Transfer (Resonant Transfer)

In this process the difference in energy between the excited and ground levels is transferred to an adjacent molecule. In the other words, two interacting molecules interchange their vibrational energy.

In the case of both of the above processes the excited level has finite lifetime ,τ, which may be described using the Heisenberg uncertainty principle:

$$\tau \approx \frac{1}{\Delta\omega_1}$$

where $\Delta\omega_1$ is the bandwith in the processes (a) and (b) described above. The broadening effect caused by these processes is called homogeneous broadening.

(c) Vibrational Dephasing.

This is frequently referred to as Pure Dephasing, or in analogy to magnetic relaxation - T_2 process. In this process, if we have a long lifetime for the excited

(a) Vibrational Energy Relaxation

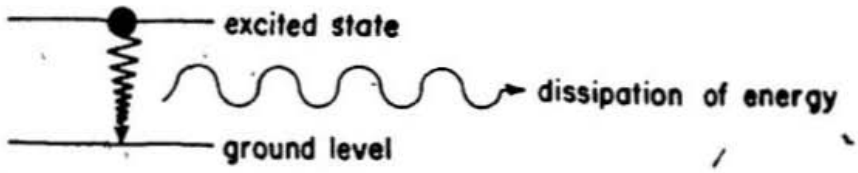

(b) Resonance Vibrational Energy Transfer

(c) Vibrational Dephasing

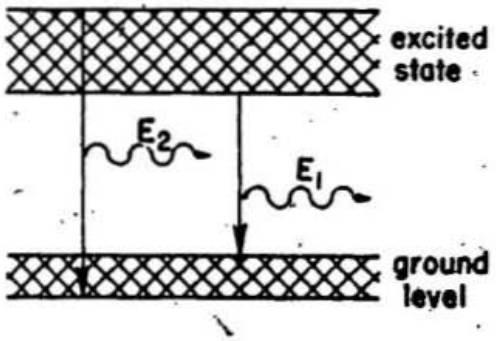

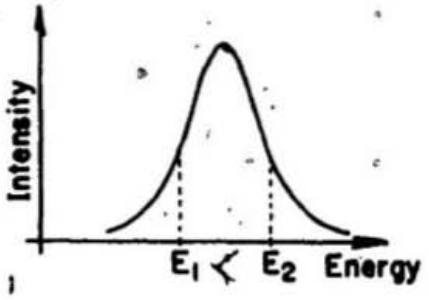

(see explanations in the text).

FIG. 6. Intermolecular interactions

energy level ($\geq 10^{-6}$sec.), then the local perturbations between the molecular oscillator of interest and the environmental molecules, cause slight shifts of the oscillator energy levels (without emission),(see Fig. 6)

$$\Delta E = E_2 - E_1 \approx \Delta\omega_2$$

where $\Delta\omega_2$ is the bandwidth due to the Vibrational Dephasing Process. In the other words elastic collisions of molecules cause modification of the phase of vibration motion, which is observed as broadening of energy levels. If the time scale of the perturbations is long compared to any other time scale of interest, this broadening is called inhomogeneous broadening. In such cases the local changes in the density of surrounding molecules are directly reflected in the broadening of the energy levels.

(d) Intramolecular Vibration-Rotation Coupling (VRC)[3,40].

In this case molecules in different rotational states have slightly different vibrational frequencies. Then rotationally inelastic collisions cause the scattering molecule to radiate at a slightly different vibrational frequency. This is properly regarded as an indirect vibrational dephasing process.

(e) Motional Narrowing[3].

For higher densities the number of inelastic and elastic collisions increases (Vibrational Dephasing and Vibration-Rotation Coupling processes occur more frequently), and different coherent contributions from the small volume elements begin to interfere. Then previously well resolved rotational components within a

band begin to overlap and collapse to the center of gravity of the unperturbed band.

The general solution of Eq. (4-5) is very difficult. This theory remains purely formal, until some approximate model is introduced for the correlation functions. The formal theory and a review of approximate models are presented in publication by Oxtoby[30]. In the next section we discuss a particular model for Vibrational Dephasing, as proposed by Rothschild[31].

5. ROTHSCHILD THEORY OF VIBRATIONAL DEPHASING

This theory is based on Kubo's stochastic treatment of line shape and relaxation phenomena[41].

Let us consider[31] a two-level vibrational system for an individual oscillator, where the lifetime of the upper vibrational level is very long, even at liquid densities. The sharp transition frequency (ω_o), which one could normally expect for this two-level oscillator is, in general, smeared out into a continuous, nonresolvable distribution of vibrational transition frequencies because of interactions between the oscillator and surrounding molecules. This results from the distribution of relative positions and orientations which cause perturbative instantaneous shifts of the lower and upper oscillator energy levels, thus leading to a "splitting" of the n-fold degenerate frequency into some distribution of frequencies around ω_o. This process is often referred to as inhomogeneous broadening.

The Hamiltonian in this case may be written in the form:

$$H = H_{oscillator} + H_{bath} + H_1(t) = H_o + H_1(t) \qquad (5\text{-}1)$$

where $H_1(t)$ is the Hamiltonian which describes coupling between oscillator and the heat bath H_o is the unperturbed Hamiltonian. Because fluctuations in the density of surrounding molecules cause changing of this coupling Hamiltonian, this part of the Hamiltonian is time-dependent.

The formalism developed by Rothschild[31] yields :

$$\langle Q(t)Q(0)\rangle \approx \exp\left\{-\frac{1}{2}\int_0^t dt' \int_0^{t'} dt'' \langle \omega_1(t'')\omega_1(t'')\rangle\right\} , \qquad (5\text{-}2)$$

where for simplicity subscripts which designate vibrational mode, and particle number are dropped and

$$\omega_1(t) = H_1(t) = \omega(t) - \omega_0 \qquad (5\text{-}3)$$

is the instantaneous oscillator energy shift caused by the perturbed Hamiltonian $H_1(t)$.

From the properties of the correlation function we obtain:

$$<\omega_1(t')\omega_1(t'')> = <\omega_1(t'-t'')\omega_1(0)> \quad , \qquad (5\text{-}4)$$

and using $\bar{t} = t' - t''$ we may define:

$$<\omega_1(\bar{t})\omega_1(0)> \equiv \Psi(\bar{t})<|\omega_1(0)|^2> \qquad (5\text{-}5)$$

where $\Psi(\bar{t})$ is the normalized autocorrelation function of the frequency shift $\omega_1(t)$ (or of the perturbation Hamiltonian $H_1(t)$). In this case Eq. (5-2) has the form:

$$<Q(t)Q(0)> = \exp\left[-<|\omega_1(0)|^2> \int_0^t d\bar{t}\,(t-\bar{t})\,\Psi(\bar{t})\right] \equiv \phi(t) \qquad (5\text{-}6)$$

and we may define the correlation times

$$\tau_c = \int_0^\infty dt\ <H_1(t)H_1(0)> = \int_0^\infty dt\ <\omega_1(t)\omega_1(0)> \equiv \int_0^\infty dt\,\Psi(t) \quad , \qquad (5\text{-}7)$$

$$\tau_a = \int_0^\infty dt\ <Q(t)Q(0)> \equiv \int_0^\infty dt\ \phi(t) \qquad (5\text{-}8)$$

Two interesting situations can be analyzed: when the perturbation coherence (correlation time τ_c) decays much slower (a) or much faster (b) than the amplitude coherence (correlation, or lifetime τ_a).

(a) $\tau_c \gg \tau_s$. In this case the perturbations, or in other words fluctuations in the density of surrounded molecules, are much slower than changes of amplitudes of the vibration molecule of the interest. We may consequently put $\Psi(t) \approx 1$ during the lifetime τ_s of $\phi(t)$. Then Eq. (5-6) simplifies to:

$$\phi(t) \approx \exp\left\{-<|\omega_1(0)|^2>\frac{t^2}{2}\right\}, \qquad (5\text{-}9)$$

and we obtain for $I(\omega)$ a Gaussian profile whose width $\Gamma = \frac{2\pi}{\tau_s}$ is determined entirely by the inhomogeneous broadening process associated with an essentially static distribution of local environments. This is referred to as the slow-motion (or static) limit, and is frequently characterized by the condition $\Gamma\tau_c \gg 1$.

(b) $\tau_c \ll \tau_s$. In this case the perturbations are very fast compared to amplitude changes of a single particle, then we may approximate $\Psi(t)$ by a delta function. By substituting $t \to \infty$ into the integration limit and from Eq. (5-6), the first integral gives $t \cdot \tau_c$ and the second integral vanishes. The result is:

$$\phi(t) = \exp\left\{-<|\omega_1(0)|^2>\tau_c\, t\right\} \qquad (5\text{-}11)$$

and $I(\omega)$ is the Lorentzian profile which is normally observed in fluids far away from the critical point. This is the so-called fast-motion limit, which is alternately characterized by the condition $\Gamma\tau_c \ll 1$; i.e. the homogeneous width $\approx \tau_c^{-1}$ is much greater than the inhomogeneous contribution.

It should be emphasized that this theory applies only to the normal fluid, where τ_c is to be associated with the first peak in the structure factor. Near a

critical point the situation is complicated by the need to consider a second, much longer correlation time, which is associated with the "slowing-down" of the hydrodynamic modes. The first theoretical treatment of this problem was proposed by Hills and Madden[42] and is discussed in the following Chapter.

CHAPTER III

CRITICAL EFFECTS

1. INTRODUCTION

The first critical point (in fluid carbon dioxide) was discovered[43] by T. Andrews in 1869. Suppose we examine a sealed glass tube containing CO_2 at an overall density of 0.48 gcm^{-3} (i.e. the critical density, ρ_C), and a number of small particles whose densities are distributed about the CO_2 value[44]. At a temperature of about 29°C (see Fig. 7), or much lower, we observe that all of the particles are floating on a sharply defined interface separating liquid from vapor. This confirms the familiar situation where the liquid and vapor densities are widely different from one another as well as from the mean value (ρ_C). At a temperature of 30°C, the interface is more difficult to detect and the least dense particles are observed to float upward into the vapor, while the densest ones sink downward into the liquid. This demonstrates that the liquid and vapor densities are more nearly the same (and almost equal to ρ_C). At 31°C the interface is hardly discernible at all, and the presence of particles at all vertical levels throughout the fluid indicates that the CO_2 density is essentially uniform from top to bottom. This constitutes the definition of the (liquid-vapor) critical point: namely, it is that well defined point in the phase diagram (see Fig. 7), where the densities of coexisting liquid and vapor converge to the same value. Careful measurements on

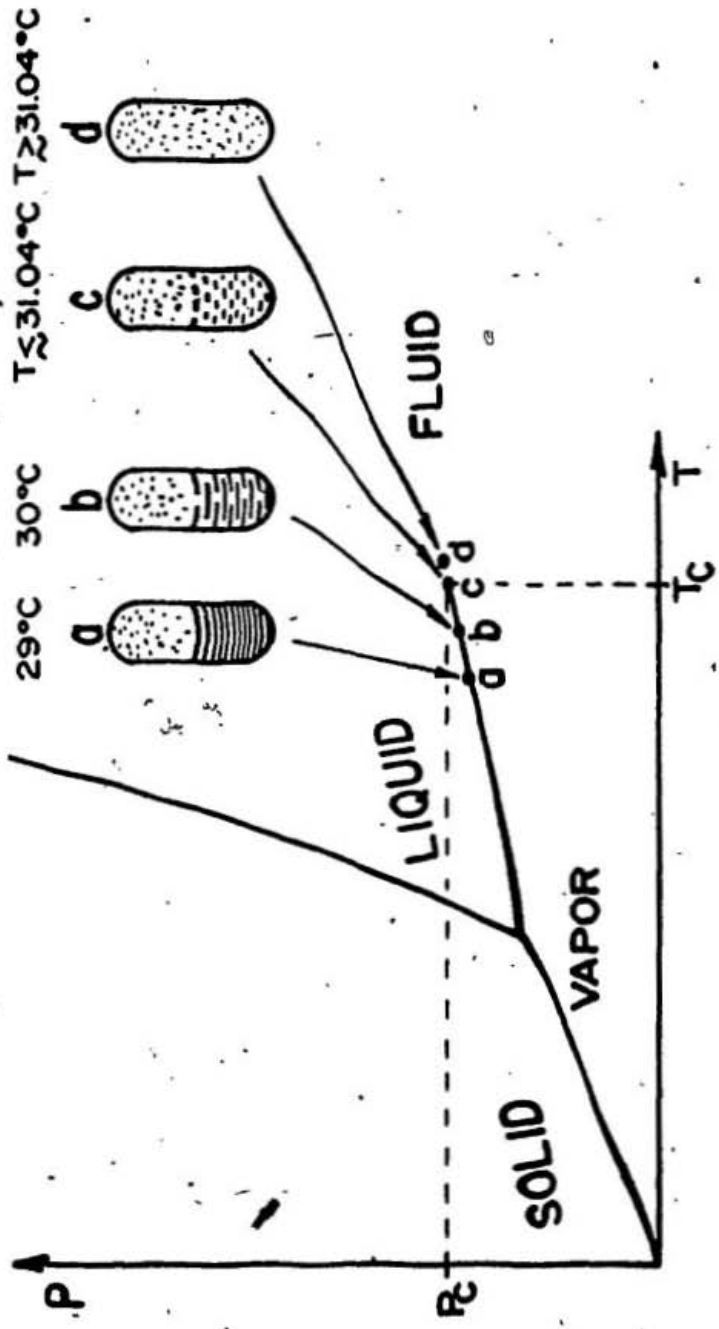

FIG. 7. Critical phenomenon in CO_2 (see explanation in the text).

CO_2 reveal that this point corresponds to $T_C = 31.04^{\circ}C$, $\rho_C = 0.48$ gcm^{-3}, and $p_C = 72$ atmospheres.

Similar phenomena have been observed in widely different systems such as[45]:

(1) near the Curie temperature in a ferromagnet like Fe (as discovered by J. Hopkinson in 1890[46])

(2) the order-disorder transition in an alloy of Cu or Zn,

(3) the transitions to superfluidity in He^4 and He^3+He^4 mixtures.

These phenomena are all characterized by the onset of large-amplitude fluctuations in one or more thermodynamic parameters as the critical point is approached.

In the case of the liquid-vapor system, which is of primary interest here, the disappearance of the interphase boundary is accompanied by the onset of microscopic fluctuations in density which pervade the entire fluid, and which render it opaque to visible light at the critical point. The scattering of visible light (critical "opalescence") has consequently been used to create advantage in studying these fluctuations[44]. Neutron and X-ray scattering have also been extensively employed to obtain information which, as for light scattering, pertains to length scales down to about 500 nm, and time scales as long as ≈ 1 μs.

The emphasis in this thesis is on the unique property of the vibrational Raman scattering process, which makes it possible to probe fluctuations in the molecular environment with a characteristic length scale of ≈ 10 nm. No

comprehensive theory has yet been developed to permit detailed interpretation of these experiments. Apart from the semi-quantitive treatments which have been described in publications from this laboratory, the work of Hills and Madden[42] is the most relevant of at most 5 publications in the field.

2. THE CRITICAL EXPONENTS AND THEORY BY HILLS AND MADDEN

In the treatment of critical phenomena it is customary to introduce the reduced temperature,

$$\epsilon \equiv \frac{T-T_c}{T_c} \tag{2-1}$$

(where T_c is critical temperature) and to invoke the well-established "universality hypothesis" which states that the important thermodynamic parameters of the system behave in accordance with power laws of the form ϵ^x. The x's are called critical exponents, and for liquid-vapor system the most important ones are identified as follows:

for density ρ;

$$\rho_{liq.} - \rho_{vap.} \approx |\epsilon|^{\beta} , \tag{2-2}$$

for specific heat;

$$C_V(T)_{liq.} \approx |\epsilon|^{-\alpha} , \tag{2-3}$$

$$C_V(T)_{vap.} \approx |\epsilon|^{-\alpha'} , \tag{2-3a}$$

for susceptibility;

$$\chi \approx |\epsilon|^{-\gamma} , \tag{2-4}$$

where

$$\chi = \frac{K_T}{K_T^0} \tag{2-5}$$

$K_T^0 = \frac{1}{\rho}$ is non-critical contribution, and $K_T = \frac{1}{\rho}\left(\frac{\partial \rho}{\partial p}\right)_T$ is the isothermal compressibility of the fluid.

As discussed in Sec. II-4 the process of Vibrational Dephasing is caused by fluctuations of density of the surrounding bath[44]. These fluctuations may be described by the correlation function:

$$<\rho(0)\rho(R)> \approx e^{-\frac{R}{\xi}} \tag{2-6}$$

where R is a specified range, and ξ is called the "correlation length". In the non-critical fluid ξ has a length of a few nm, but in the vicinity of the critical point it becomes very large ($\approx$ 1 μm) and becomes comparable with the wavelength of visible radiation. The medium will then contain fluctuations or inhomogeneities on that scale, and this will give rise to strong scattering, i.e. to the critical opalescence (unusual strong intensity of scattered light). When we introduce the inverse correlation length, $\kappa = \frac{1}{\xi}$, then another critical exponent is defined via the relation:

$$\kappa = \kappa_0 \epsilon^{\nu} \tag{2-7}$$

which, consequently, is expected to be of importance in understanding the behaviour of near-critical spectra.

A similar power law also holds for the thermal diffusitivity, D_T, i.e.:

$$D_T \overset{\nu-1}{=} D_T^0 \epsilon^{\gamma-\alpha} \tag{2-8}$$

where D_T^0 is thermal diffusitivity in the non-critical region.

A theory for determining values of critical exponents from vibrational Raman data was first given by Hills and Madden[42], under the basic assumption that pure dephasing (PD) was the only significant line broadening mechanism. They used an approach similar to that applied in neutron scattering[45], and X-ray scattering[47]. Namely, the rate of vibrational dephasing of molecules in a liquid is regarded as being determined (i) by the dynamical structure of the fluid, $S(k,\omega)$, which is the Fourier transform of the density-density correlation function and (ii) by a probe-fluid potential, $V(k)$, which effectively picks out those k-Fourier components of the density fluctuations, that are most effective in causing the dephasing. The frequency dependence of the scattering intensity is then described by:

$$I(\omega) \approx \rho_e \int_0^\infty dk\ k^2\ S(k,\omega)\ V^2(k), \tag{2-9}$$

where ρ_e is the equilibrium liquid density, and ω is spectral linewidth. The dephasing rate is thus expressed as an integral of the dynamical structure factor $S(k,\omega)$ over all k-Fourier components weighted by $V^2(k)$.

Assuming fast-modulation conditions to apply, Hills and Madden showed that the PD contribution to the linewidth could be written as

$$\Gamma_{PD} = 2\rho\ \lim_{\omega\to 0} \sum_L B_L \int_0^\infty k^2 dk\ S(k,\omega) V_L^2(k)\ , \tag{2-10}$$

where L characterizes the manner in which the interaction transforms under rotation.

An important simplifying assumption made in this treatment was to regard the density fluctuations as being characterized by two distinct time scales. First, there are the normal, or non-critical, fluctuations which are associated with the first peak in the structure factor. In this case the time scale is $\approx$ 1 ps and, with experimental support from other sources[17], the associated contribution (Γ^0_{PD}) to the linewidth is not expected to exhibit any critical effect. Second, there are the hydrodynamic fluctuations which are in fact responsible for the critical phenomenon, and which are characterized by a time scale as long as $\approx$ 1 μs. The effects observed near the critical point are thus associated entirely with the latter broadening contribution (Γ'_{PD}), and the two contributions are regarded as additive:

$$\Gamma_{PD} = \Gamma^0_{PD} + \Gamma'_{PD} \quad . \tag{2-11}$$

The problem is then reduced to determining the behaviour of Γ'_{PD}.

From classical hydrodynamics, the (Ornstein-Zernicke) structure factor for hydrodynamic fluctuations near a critical point is given by

$$\frac{1}{\rho_e} S_{HYD}(k,\omega) = \frac{K_T}{K_T^0} \frac{\kappa^2}{\kappa^2+k^2} \frac{1}{\pi} \frac{\tau}{\omega^2+\tau^2} \tag{2-12}$$

where $\tau = D_T k^2$, $D_T = \frac{\lambda'}{\rho_e c_p}$, λ is thermal wavelength, and c_p is specific heat at constant pressure.

Assuming that on approaching the critical point $V(k) \approx V(0) \approx$ const, we may solve Eq. (2-9), and in the end obtain the contribution to the spectral width

from the long-range hydrodynamic modes of the fluid, i.e.

$$\Gamma'_{PD}(\omega) \approx \frac{K_T}{K_T^0}\,\kappa^3 \left\{ \frac{\phi}{\omega^2+\phi^2} + \left(\frac{|\omega|}{2\phi} \right)^{\frac{1}{2}} \frac{\omega-\phi}{\omega^2+\phi^2} \right\} \qquad (2\text{-}13)$$

where : $\phi = \kappa^2 D_T$.

Two cases are now considered. In the case (I), where $\omega \ll \phi$ (the case further from the critical point, where the correlation length is very short and linewidth ω is small), then Eq. (2-12) reduces to the form:

$$\Gamma'_{PD}(\omega) \approx \frac{K_T}{K_T^0}\,\frac{\kappa}{D_T} \qquad (2\text{-}14)$$

Eqs. (2-5), (2-7), (2-8) then yield

$$\Gamma'_{PD}(\omega) \approx \epsilon^{-2\gamma+\nu+a} \qquad (2\text{-}15)$$

Taking values for $\gamma = 1.25$, $\nu = \frac{2}{3}$ and $a = 0.52$, which are obtained by the three dimensional Ising model, or from experimental measurements[48,49], the authors[42] obtain:

$$-2\gamma + \nu + a \approx -1.31 \qquad (2\text{-}16)$$

For the case (II) $\frac{\omega}{\phi} \gg 1$, or $\omega \ll \phi$, (in the vicinity of the critical point, correlation length long) Eq. (2-9) reduces to

$$\Gamma'_{PD}(\omega) \approx \frac{K_T}{K_T^0}\,\kappa^2 (2\omega D_T)^{-\frac{1}{2}}, \qquad (2\text{-}17)$$

so that

$$\Gamma'_{PD}(\omega) \approx \epsilon^{-\frac{3}{2}\gamma+2\nu+\frac{a}{2}} \tag{2-18}$$

Again, the above critical exponent values[48,49] give

$$-\frac{3}{2}\gamma + 2\nu + \frac{a}{2} \approx -0.28 \tag{2-19}$$

In the region very close to the critical point, Hills and Madden also consider the special case (III) where a transition to slow-motion conditions occurs and Eq. (2-9) does not apply. This case is called the "statistical" or "rigid-lattice" limit, and the spectrum I(ω) simply reflects a time-independent distribution of local environments in the fluid. The Hills and Madden result for this case is

$$\Gamma'_{PD} \approx \frac{K_T}{K_T^0}\kappa^2 , \tag{2-20}$$

$$\Gamma'_{PD} \approx \epsilon^{-\gamma+2\nu} , \tag{2-21}$$

$$-\gamma + 2\nu \approx 0 \tag{2-22}$$

Hills and Madden point out that the assumption of fast-motion conditions is appropriate for liquids N_2 and O_2 because experimental data[15] show the Raman spectra to be highly Lorentzian unless the critical point is approached very closely. They also showed, that the linewidth data[15] were consistent with case (II), i.e. Eq. (2-18), which is the most plausible for the given experimental conditions. On this basis they claimed support for the validity of their theory.

In a subsequent publication[17] Clouter *et al.* questioned the appropriateness of using the data for N_2 and O_2 as a testing ground for this theory. They cited

evidence which indicated that the Raman linewidth in these liquids involved contributions from other than the pure dephasing mechanism so that the basic assumption of Hills and Madden could be seriously compromised. New data for the totally symmetric mode of CH_4 were proposed as a more clear-cut test case, and it was demonstrated that agreement with the theory could be obtained by using a more realistic form for the structure factor, than the simplest hydrodynamic model. This provided a consistent interpretation of the data for all three systems.

The Hills and Madden theory should consequently be regarded as a moderately successful first attempt which is applicable only in the minority of cases where pure dephasing is the exclusive mechanism. As will be discussed later, in the HD case pure dephasing appears to be sufficiently dominant for this theory to apply.

CHAPTER IV

APPARATUS AND EXPERIMENTAL PROCEDURE

1. EXPERIMENTAL ARRANGEMENT

The experimental set-up has been described in more detail in a number of theses and publications (for example Ref. 20, 50, 51). Therefore only a brief description will be given below.

The sample cell was made from a Be-Cu alloy, which is characterized by high tensile strength as well as high thermal conductivity. The former property was required for containment of the high pressure ($\leq$ 1000 bars), while the latter property was required in order to minimize temperature gradients within the near-critical samples. The construction of the cell is shown[20] in Fig. 8. The mass of the cell is about 1 kg, and its internal volume (0.5 cm^3) consists of two mutually perpendicular and intersecting bore holes of 3.2 mm diameter. They are closed by quartz windows (w) of 3.2 mm thickness and 10 mm diameter. The remaining hole at the top of the cell was connected to the external gas-handling system through an isolation valve (v), whose closure point was located about 1 cm above the scattering volume.

Cooling was achieved by conduction through a copper block (not shown in Fig. 8) which was clamped to the cell and to the second-stage cold head of closed-cycle He-gas cryogenerator (Air Products CSA-202). The cell was placed in

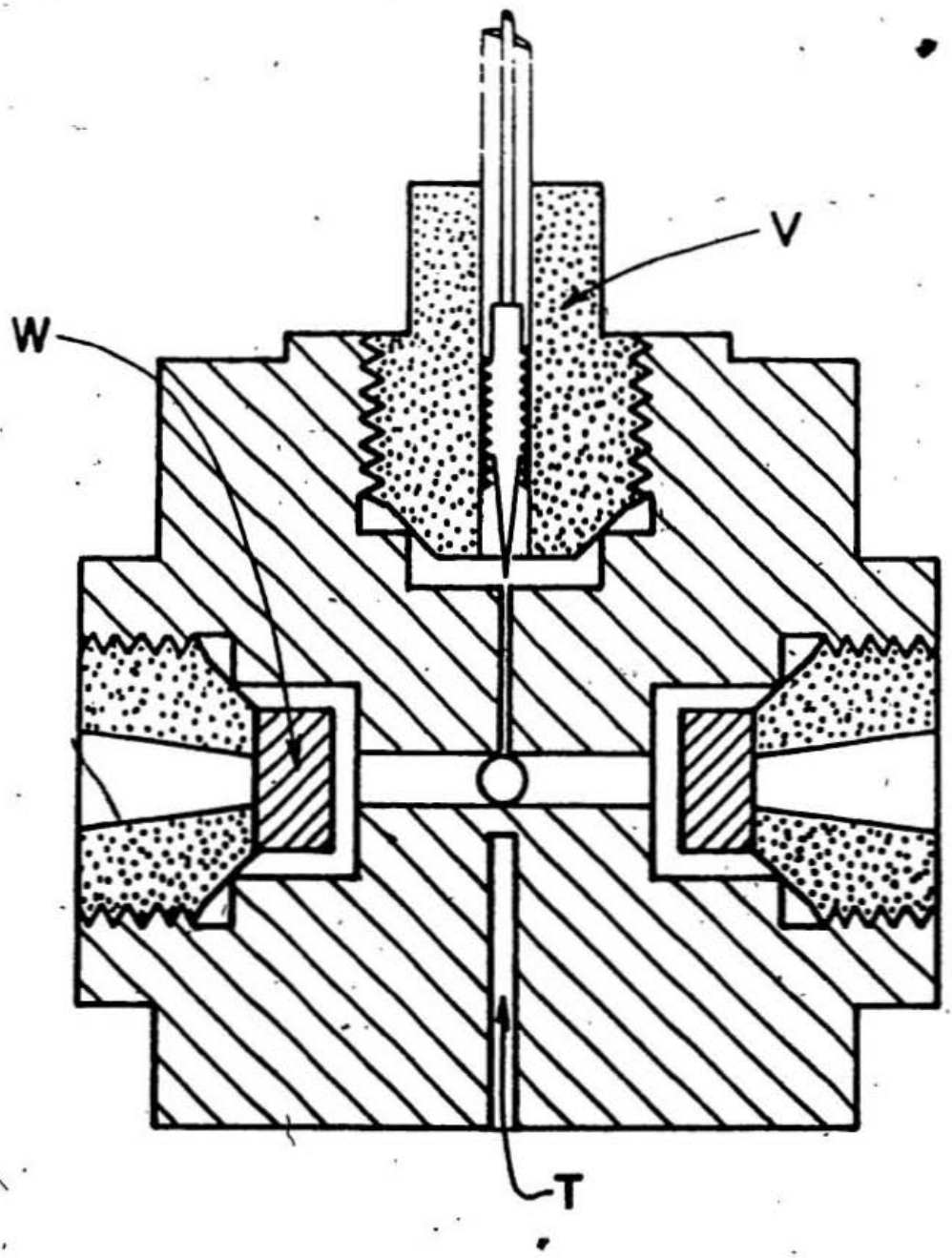

FIG. 8. Be-Cu sample cell. V is the isolation valve, T the carbon thermometer well, and W the quartz window (Ref. 20).

a vacuum insulated chamber with an intermediate radiation shield which was kept at a temperature approximately 50 K above that of the cell by thermal connecting to the first-stage cooling element of the cryogenerator. Fine temperature control was provided by (1) a calibrated carbon resistance thermometer placed in the thermometer well T in Fig. 8, (2) two 20 Ω heaters, which were connected in series and mechanically clamped to the body of the cell, (3) a programmable digital ohmeter (Fluke 8860A), and (4) a power amplifier. The ohmeter was programmed to compare the resistance of the carbon thermometer with a preset reference value, and to send an appropriate correction signal to the power amplifier, which was capable of delivering a maximum power of about 2 W to the cell heaters. The overall arrangement was characterized by a thermal response time of about 30 s, and provided long-term control which was stable to within 0.01 K under optimum conditions.

The overall arrangement of the apparatus is shown in Fig. 9 (Ref. 20). The exciting radiation was provided by an Ar^+ laser (Spectra Physics 165-08), operating in a single cavity mode with a nominal wave length of 514.5 nm, and a power output of 300-500 mW.

The spectrometer consisted of a scanning Fabry-Perot (FP) interferometer (Burleigh RC-110), a cooled photomultiplier (PMT) detector (ITT FW 130), photon counting electronics, and a combined data-acquisition plus Fabry-Perot control system (Burleigh DAS-1). The spectra were acquired by a process of repetitive scanning with a period of about 10 s, and the total accumulation time

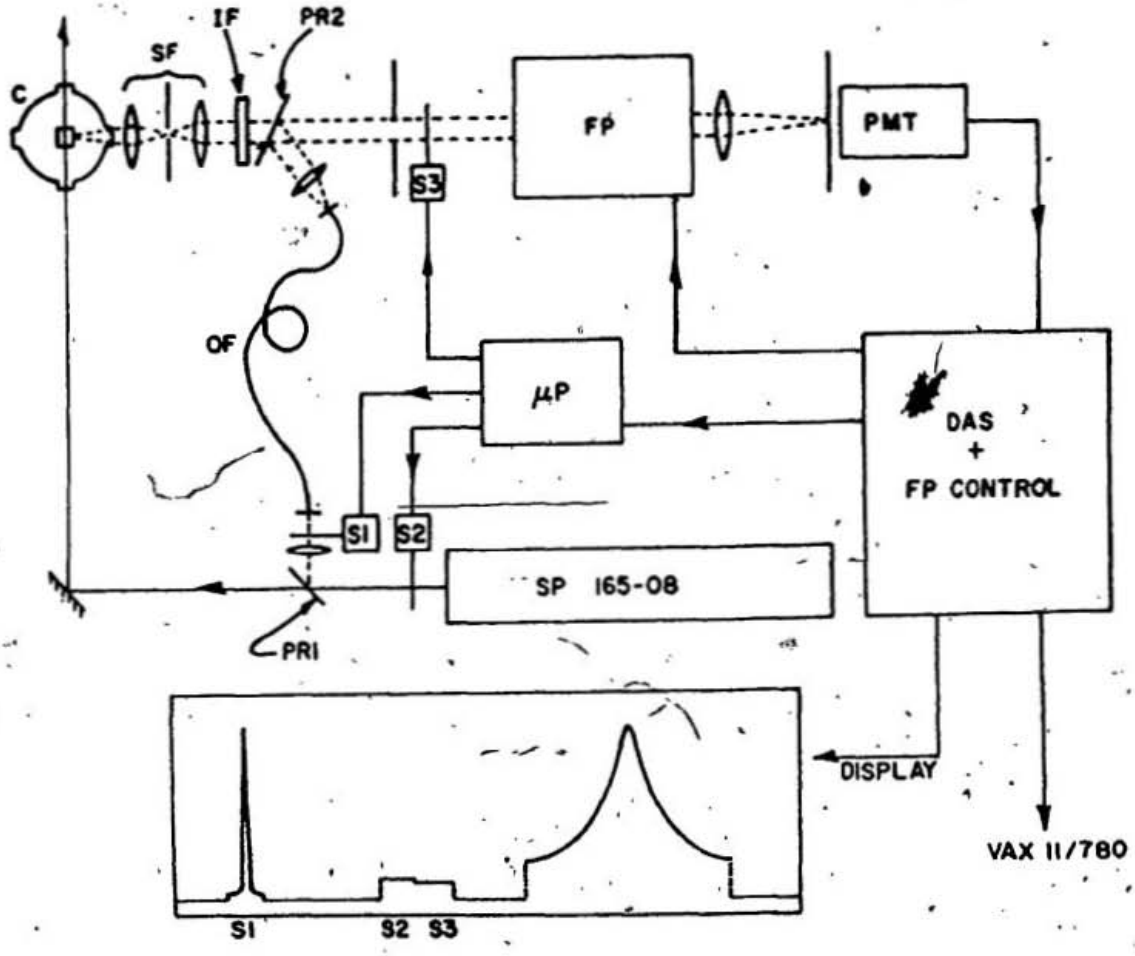

FIG. 9. Schematic diagram of the experimental setup. C is the cryostat; SF the spatial filter; PR1 and PR2 the uncoated glass reflectors, S1, S2 and S3 the electromechanical shutters (S3 shutter was not used in experiment with the HD), FP the Fabry-Perot interferometer, PMT the cooled photomultiplier tube, OF the optical fiber, μP the microprocessor, DAS the data acquisition system, and SP the Ar^+ laser (Ref. 20).

required to achieve acceptable signal-to-noise ratio was 3 to 24 hours. It was consequently necessary to fully utilize the feedback control capability[20] of the DAS in order to minimize the effects of long term drift in the interferometer alignment. The reference signal recquired for this purpose would normally be the parasitic Rayleigh peak which was eliminated by filtering in this experiment (filter IF in Fig. 9). The required alternative arrangement (Fig. 9), utilized an uncoated glass reflector, PR1, to deflect a sample of the laser output through an optical fiber (OF) when the shutter S1 was open. The light which emerged from the fiber was collimated and accurately directed, by uncoated glass reflector PR2, along the axis of the scattering optics. The action of shutter S1 was controlled by a microprocessor (μP) which utilized the master clock of the DAS as a time base. S1 was programmed to open at a point nearest the beginning of each sweep, where resonant transmission of the laser frequency was about to occur, and it was closed immediately afterward, so that no laser radiation reached the detector during scanning of the Raman line. The microprocessor also controlled shutter S2 which was used to monitor the ambient background during the "beam-off" condition. A representative display, as it would appear on the CRT screen of the DAS, is shown at the bottom of Fig. 9. Data were transmitted from the DAS to a Tandy 1200HD computer and stored for further processing as described in section 3.

2. SAMPLE PREPARATION

Experiments were performed along three constant density (isochoric) paths, corresponding to bulk density ($\bar{\rho}$) values of $0.504\rho_C$, ρ_C, and $2.25\rho_C$. The critical density of 357 amagat[52,53] was established by first filling the cell with liquid at a temperature about 0.1 K below that where the interphase boundary disappeared. Material was then extracted from the cell in stages until (with the liquid level at approximately the half-height point) it was observed that the interface disappeared without vertical movement as the temperature of the isolated sample was slowly raised. This method was quite accurate and did not require precise determinations of either pressure or temperature.

In order to establish other sample conditions it was necessary to obtain information for HD densities at temperatures between 25 K and T_C. Since no such data were available in the literature, it was decided to apply the methods proposed by Rudenko and Slyusar[54,55]. They pointed out that for the same reduced temperatures, ϵ, the densities of H_2 and D_2 were simply related through a constant of proportionality. From available experimental data for normal H_2 and D_2 they determined $\rho_D/\rho_{H_2} = 2.25$ (where ρ is in g/cm^3), and predicted that a similar procedure should apply for HD. Present calculations, using data in the range from 16.6 K to 25 K, yielded the consistent ratio $\rho_{HD}/\rho_{H_2} = 1.58\pm0.02$. This value predicted a critical density of 355 amagat (at $T_C = 35.91$ K) as compared with the experimental value[52,53] of 357 amagat. This agreement was considered to be acceptable so that the densities of liquid and vapor HD were

subsequently determined (for given ϵ) by multiplying known normal H_2 densities[54,55] by 1.58.

The condition for the lower density isochore were now established by starting with the cell partly filled with liquid at 34.64 K. Gas was removed from the cell until the liquid just disappeared completely, and the density of the remaining vapor was calculated as above to be 180 amagat or $0.504\rho_C$. Similarly, the higher isochore density of 803 amagat ($2.25\rho_C$) was obtained by carefully closing the valve when the cell was completely filled with liquid at 26.19 K. This method was convenient because it did not require precise measurements of the pressure.

The HD gas used in the experiments was acquired commercially (from Merck, Sharp, and Dohm) with its principal impurities being isotopic variants H_2 and D_2. The level of each of these impurities was estimated from the intensities of their vibrational Raman spectra to be approximately the same, and it was concluded that the minimum HD content was 93%. While it was considered unlikely that these impurities would have any significant effect on the HD Raman spectra, they probably account for the fact that the value of T_C as determined in the present experiments was 0.37 K higher than the published[52,53] value (35.91 K) for pure HD. The observed increase in this value is consistent with the method (above) by which the critical condition was established. Since the temperatures involved in this process were greater than T_C for H_2 (33.00 K) while below T_C for D_2 (38.3 K), it is reasonable to expect that fractional distillation would enhance the latter impurity at the expense of the former and thereby give rise to

a slight increase in T_C. At the same time it should be noted that this method for determining T_C is a definitive one, and no alternative was available. Throughout the remainder of this thesis it should therefore be assumed that the appropriate value for T_C is 36.28 K.

3. DATA ANALYSIS

The 512-channel output from the DAS was processed on a Tandy personal computer, using programs orginally written by M.J. Clouter for use on the university Vax system, and modified by R. Craig for the Tandy. The first stage involved three steps, which may be briefly described as follows[20]:

(1) An average background level was calculated from the 490 to 510 channel signal provided by shutter S2. This value was stored for later use, together with other manually entered parameters such as free spectral range (SFR), temperature, pressure, etc.

(2) The data for the instrument function, as provided by shutter S1 was processed by a least-squares routine which yielded a two-parameter fit to the theoretically predicted Airy function:

$$S_I(\nu) = \frac{C_1}{[1+C_2\sin^2(\frac{\pi\nu}{R})]} , \qquad (3\text{-}1)$$

where C_1, C_2 are the adjustable parameters, which determine peak height and width, respectively. R is the known spectral free range (SFR), of the interferometer, and ν is the frequency relative to the peak of the profile.

(3) After this operation only about 200 points comprising the Raman spectrum were retained, with appropriate channel identifiers for recovering the position of the spectrum relative to the peak of the laser reference line. The remaining data from the DAS output were discarded.

The second stage of the data processing made corrections for the finite instrument resolution. In this case the following steps were performed:

(1) The three-point smoothing routine was applied to the Raman data, in order to reduce the undesirable effects of high-frequency noise (see Fig.10a and b).

(2) The wings of the spectrum sometimes contained extraneous information. For example, in the Fig. 10a there appears a weak higher order of the laser line which was not completely removed by the optical filter (IF in Fig. 9) used in the experiment. Such features were removed by truncating the tails of the spectrum, and an Airy function extrapolation was used to generate the interorder minima. 15 to 60 points from original spectrum were used to generate these new tails.

(3) A smoothing operation was once again applied to the spectral wings, where high-frequency noise was removed by using an n-point ($n < 10$) averaging process. This process was weighted so that its effectiveness was maximum at the extremes of the data, while falling rapidly to zero at a point about 0.3 R from the peak on either side. The result of these processes is shown in Fig. 10c.

4) The observed spectrum $S_O(\nu)$ and the "true" spectrum $S(\nu)$ are connected by a relation which involves the instrumental function $S_I(\nu)$:

$$S_O(\nu) = S(\nu) * S_I(\nu) \ , \qquad (3\text{-}2)$$

where * signifies the mathematical operation of convolution. The Fourier transform of above equation reduces it to the simple form:

$$F[S_O(\nu)] = F[S(\nu)]\, F[S_I(\nu)] \ , \qquad (3\text{-}3)$$

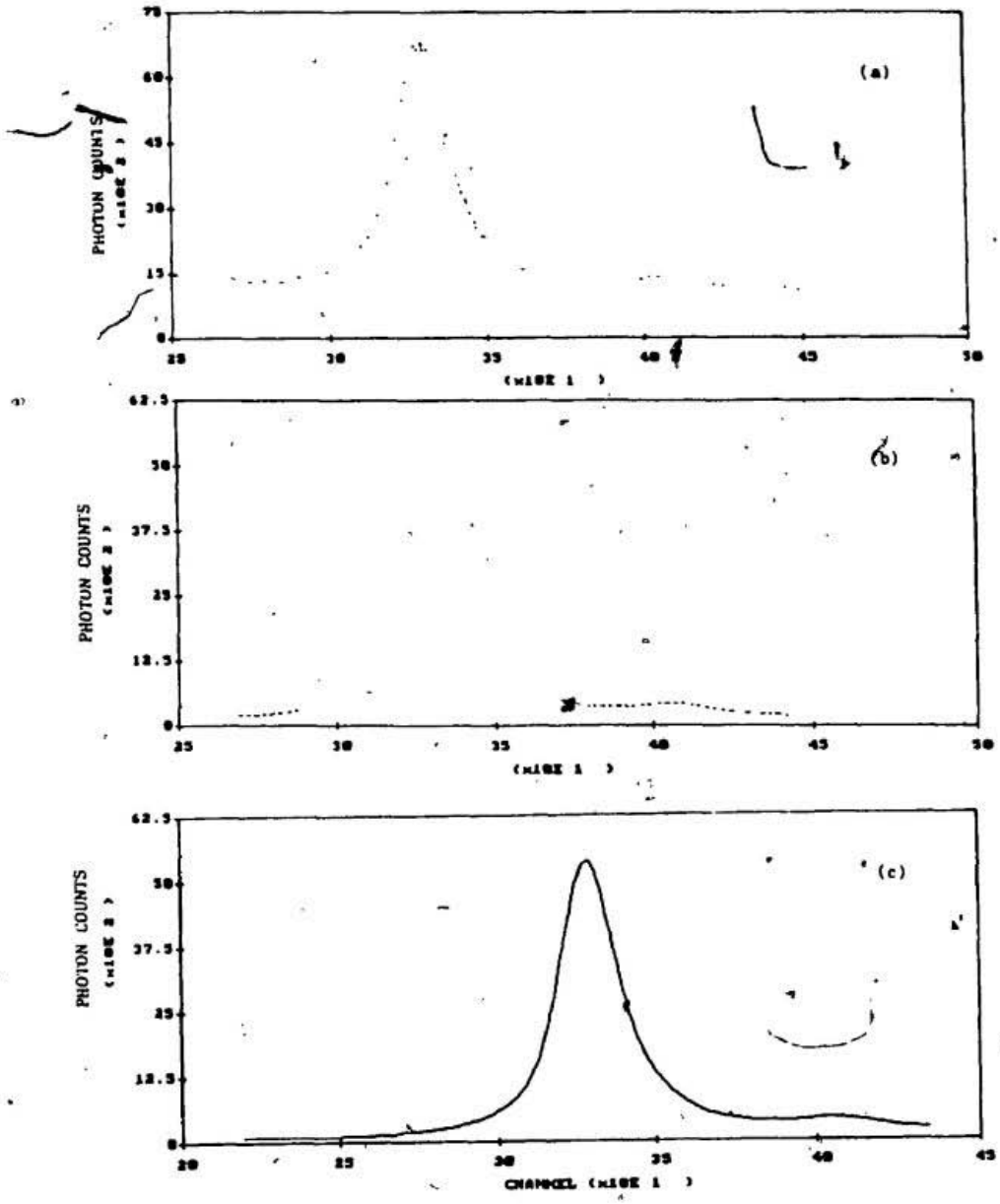

FIG. 10. The Q-branch of HD vapor at 32.3 K.

(a) observed on the screen of the DAS-1,

(b) after substracting the background, triming the tails of spectrum, and three-point smoothing,

(c) after fitting the Airy function to the tails of the spectrum,

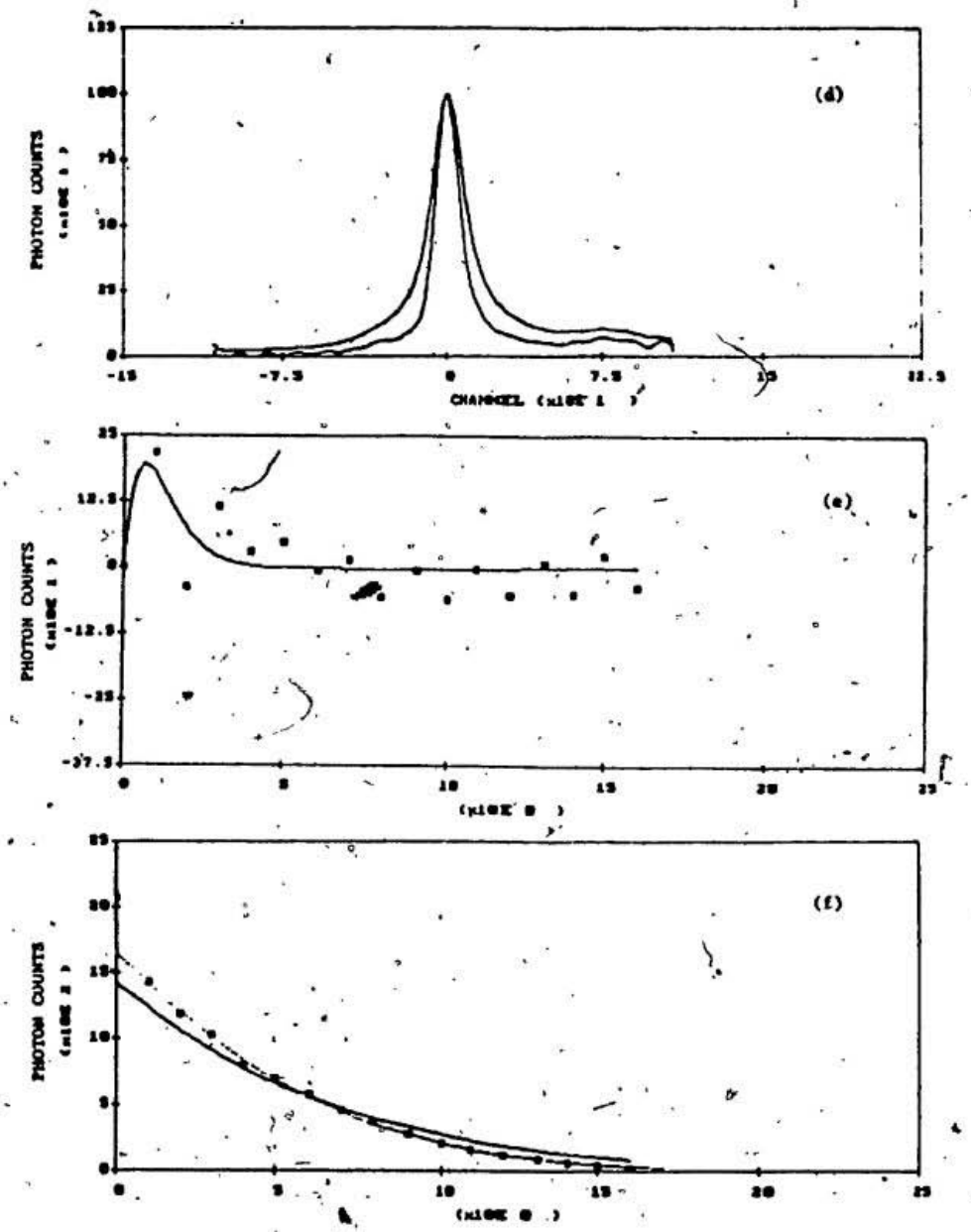

FIG. 10. The Q-branch of HD vapor at 32.3 K.

(d) the spectrum from (c) compared with the spectrum after deconvolution,

(e) sine coefficients of the Fourier transformation,

(f) cosine coefficients of the Fourier transformation (dotted line is final fit, and solid line is first approximation).

or,

$$\mathcal{I}_O(t) = \mathcal{I}(t)\ \mathcal{I}_I(t) \quad , \tag{3-3a}$$

The recovery of the "true" spectrum by a process of deconvolution is then achieved by the relatively trivial operation:

$$\mathcal{I}(t) = \mathcal{I}_O(t)/\mathcal{I}_I(t) \quad , \tag{3-4}$$

and $S(\nu)$ was obtained directly as the inverse transform, of $\mathcal{I}(t)$. Since the instrumental function was symmetrical, its transform consisted simply of a set of cosine coefficients $A_{I,n}$, which were obtained directly from the analytical solution:

$$A_{I,n} = \left[1+\frac{2}{C_2}\left[1-(1+C_2)^{\frac{1}{2}}\right]\right]^n \quad , \tag{3-5}$$

with n=0,1,2,...

Because the S_O profile was generally asymmetric, so that the corresponding Fourier series included both cosine ($A_{O,n}$) and sine ($B_{O,n}$) terms. The number of terms required was determined by a visual comparison (on a video terminal screen) of the inverse transform with the smoothed data. In general it was not possible to distinguish between the two superimposed displays with n in the range $6 \leq n \leq 20$.

The deconvolved ("true") spectrum S was thus obtained from a Fourier series with coefficients given in accordance with Eq. (3-4) as $A_n = A_{O,n}/A_{I,n}$, and $B_n = B_{O,n}/A_{I,n}$. Fig. 10d shows a comparison between profiles for S_O and

S. The spectrum taken for illustrating these procedures (Fig. 10) was narrow, and the instrument resolution had a significant effect on the spectrum. For most data this effect was much smaller.

As distinct from the case of previous N_2 experiments[20], this stage of the data processing was complicated by the overlapping of two Raman lines corresponding to the $Q_1(0)$ and $Q_1(1)$ transitions. This placed additional demands on the accuracy of the deconvolution process, and is responsible for the extraneous oscillations which are evident in Fig. 10d. This was not a serious problem, however, because emphasis was placed on the recovery of $Q_1(0)$ data. The $Q_1(1)$ feature, whose intensity was temperature dependent, was always quite weak and sometimes undetectable. The consequences were, however, somewhat more serious in the (following) final stage of data processing.

In the last, (third) stage of the data analysis, attempts were made to represent the deconvolved spectra in terms of analytic functions[19,20]. For the single (isolated) Raman line these functions are theoretically[31,42] predicted as Gaussian, Lorentzian or Voigt profiles (the Voigt profile is obtained by convolution of Gaussian and Lorentzian functions). The Fourier transform of the Voigt function is as follows:

$$A(t) = F[L(\nu) * G(\nu)] = v_0 \exp(-v_1 t - v_2 t^2) \quad . \qquad (3\text{-}6)$$

(see Fig. 10f). The A_0 coefficient was excluded from the fitting procedure. This discriminated against the presence of any broad-band signals which were not part of $Q_1(0)$ spectrum[20]. In some cases it tended to "wash out" the weak $Q_1(1)$

component in the tail of the spectrum, but the $Q_1(0)$ profiles were reproduced correctly. For the cases where overlapping of the $Q_1(0)$ and $Q_1(1)$ components was strong, the spectra obtained by this procedure were in excellent agreement with the original spectra.

Highly symmetric, non-critical spectra were represented by a periodic superposition of Voigt profiles, $V(\nu)$, with the periodicity R required by the Fabry-Perot interferometer :

$$S(\nu) = \sum_{-\infty}^{\infty} V(\nu + mR) \ , \qquad (3\text{-}7)$$

where the sum is over the integer m. The $V(\nu)$ functions were obtained as the inverse transform of A(t), which was least-squares fitted to the experimentally determined cosine coefficients for each (symmetric) spectrum.

The spectra for HD vapor near the critical point, and corresponding spectra on the critical isochore were highly asymmetric. In these cases, as was done for the spectra of N_2^{20}, the required sine coefficients were represented by the empirical form,

$$B(t) = b_0 \exp(-b_1 t)\sin(b_2 t) \ , \qquad (3\text{-}8)$$

where the b_i parameters were again determined by least-squares fitting (see Fig. 10e). The inverse transform, using both the fitted functions A(t) and B(t), produced the more general profile, $I(\nu)$, corresponding to a single period of the Fabry-Perot spectrum. The entire Fabry-Perot spectrum could then be generated by a periodic superposition analogous to Eq. (3-7).

The $S(\nu)$ functions were introduced because they permitted calculation of a better approximation to the isolated Raman spectrum. In principle, the effect of inter-order overlap, which is characteristic of the Fabry-Perot interferometer, can be reduced (or even eliminated) by generating additional Fourier coefficients from the fitted A(t) and B(t) functions via interpolation. If the number of coefficients is increased by a factor of 5, for example, it has the effect of expanding the $S(\nu)$ period by the same factor, i.e.

$$S(\nu) = \sum_{-\infty}^{\infty} I(\nu + 5mR) \quad , \tag{3-9}$$

and thereby reduces the overlap in the wings of $I(\nu)$. The validity of this procedure is determined by the accuracy with which A(0) is known, and in the present case this accuracy could not be assessed. The procedure was nevertheless carried out on the grounds that it should produce a better approximation to the true spectrum than $I(\nu)$ itself.

CHAPTER V

DISCUSSION OF RESULTS

1. GENERAL REMARKS

The first vibrational quantum of HD has an energy of about 3812 cm^{-1} and (as also for H_2 and D_2) it is only at temperatures well above room temperature that the anti-Stokes (deexcitation) spectra corresponding to $v=1 \rightarrow v=0$ are observable. All the HD spectra which are to be discussed (Figs. 11a-e) are consequently Stokes (excitation) spectra arising from $v=0 \rightarrow v=1$ transitions, and the scattered radiation involved was red shifted to $\approx$640 nm from that of the exciting laser line (at 514 nm). It was not possible to measure this (absolute) shift with any accuracy using a Fabry-Perot interferometer so that relative shifts only are referred to in the following discussion.

In addition, since all spectra were obtained at temperatures below 60 K, only the J=0 and J=1 rotational levels (of the ground vibrational state) were significantly populated. Calculations[52] show that at 30 K the relative populations of these two levels are 0.96 and 0.04, respectively, so that the Q(0) transition can be expected to dominate while the Q(1) feature is only marginally observable. The effect of temperature on the spectrum is demonstrated by the results of Witkowicz and May[7] which are reproduced in Fig. 12 for room temperature (300 K) and 85 K. The present spectra are similar to their latter results with the

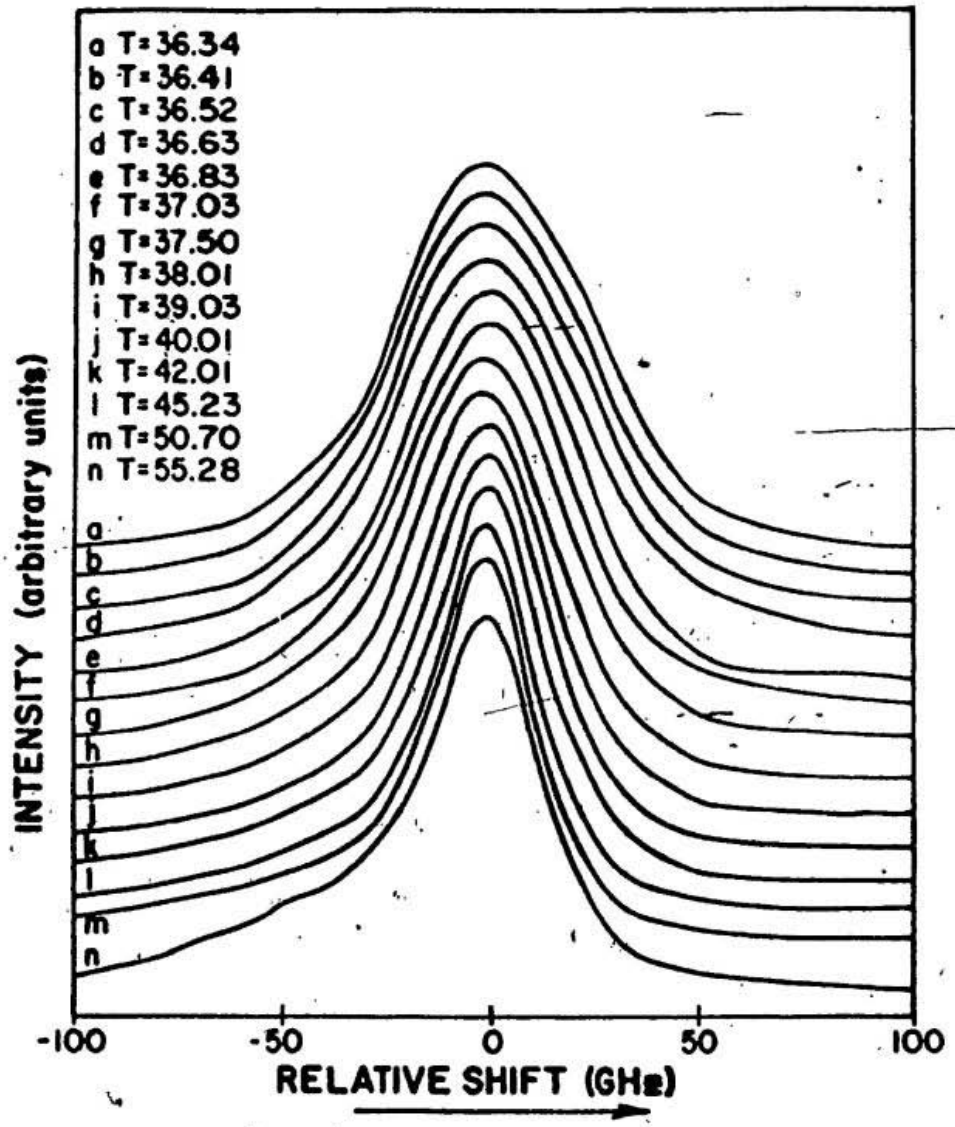

FIG. 11a. The Q-branch of gaseous HD at different temperatures (in Kelvins) along the critical isochore (ρ_C = 357 amagat, SFR=215 GHz).

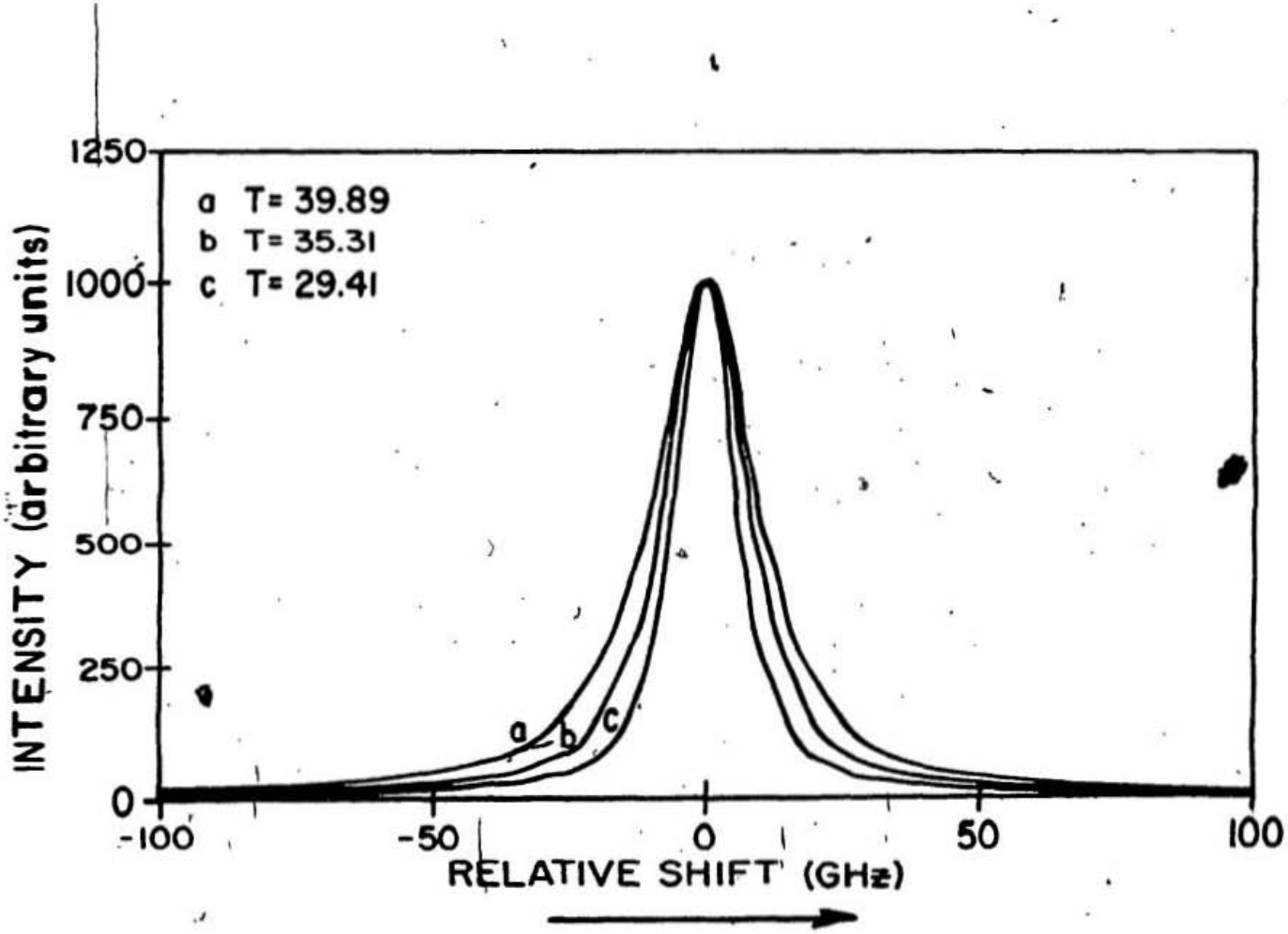

FIG. 11b. The Q-branch of gaseous HD at different temperatures (in Kelvins) along isochore $\rho = 2.25\ \rho_C$ (SFR=117 GHz).

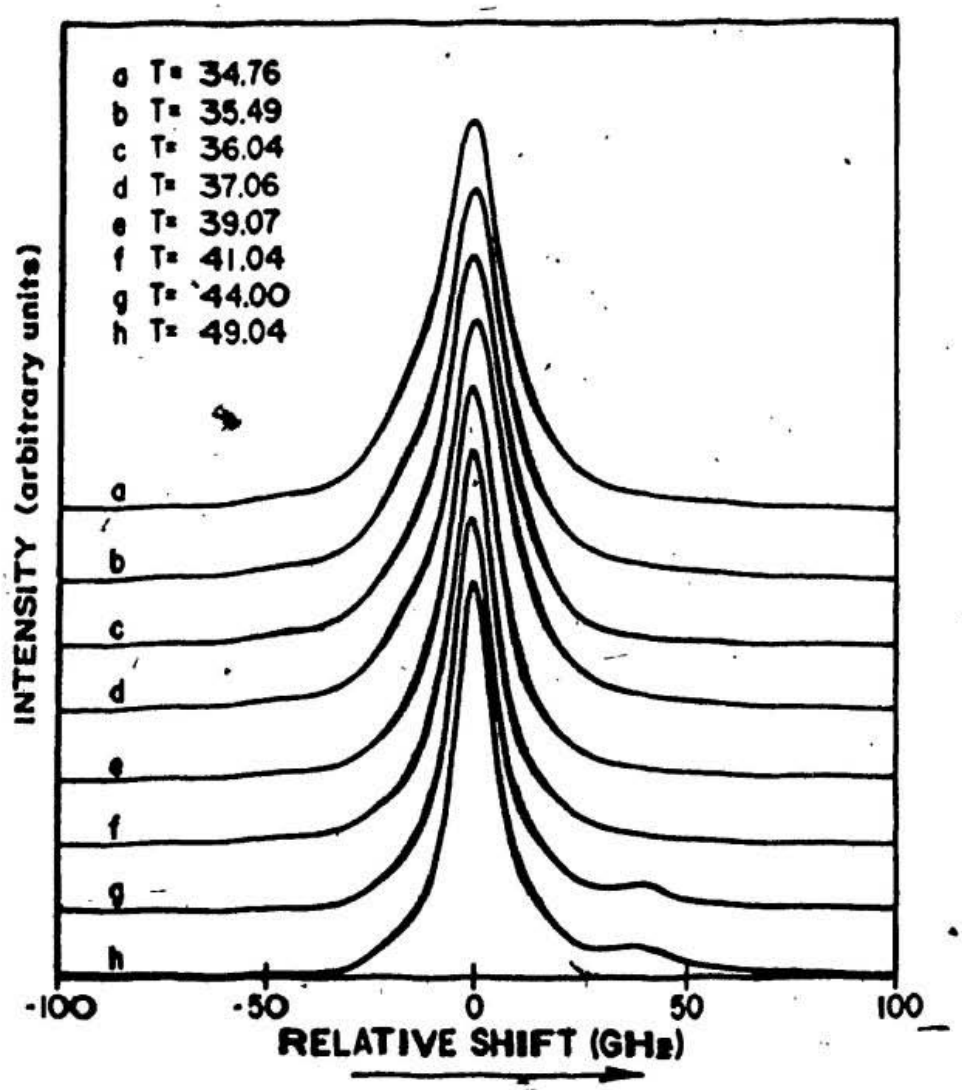

FIG. 11c. The Q-branch of gaseous HD at different temperatures (in Kelvins) along isochore $\rho = 0.504\,\rho_C$ (SFR=117 GHz).

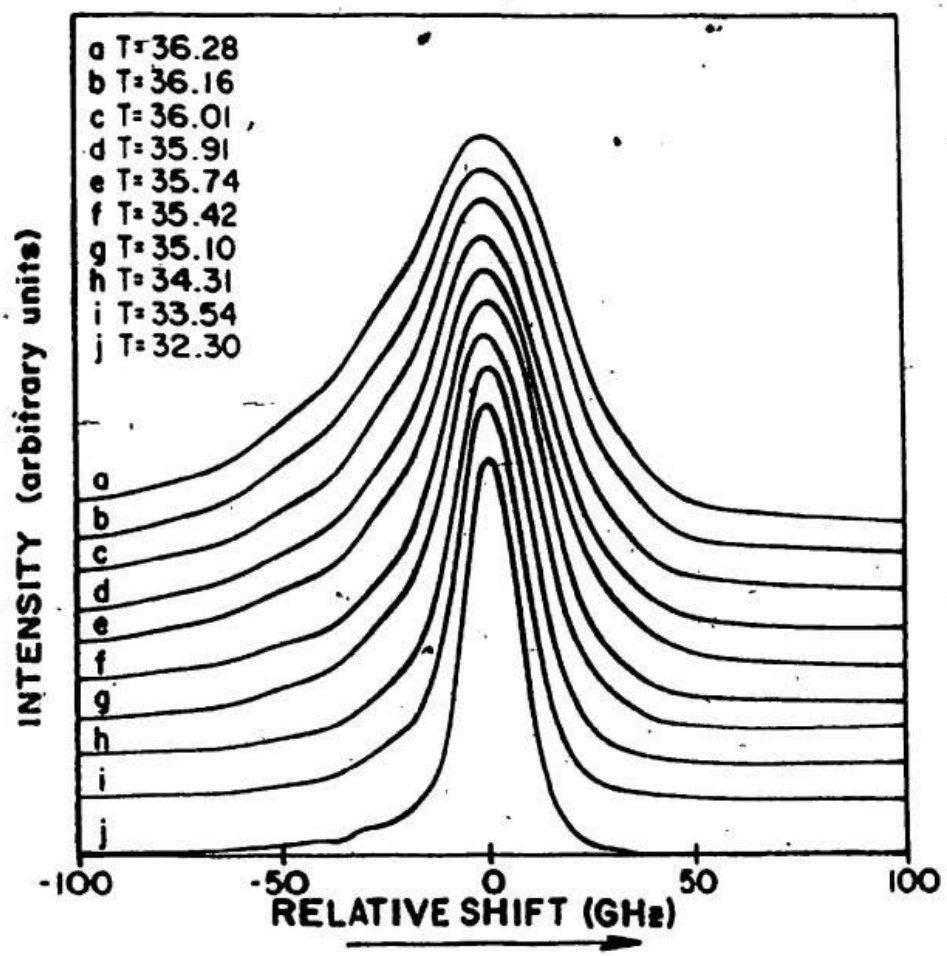

FIG. 11d. The Q-branch of HD vapor along the vapor-liquid coexistence curve (SFR=215 GHz).

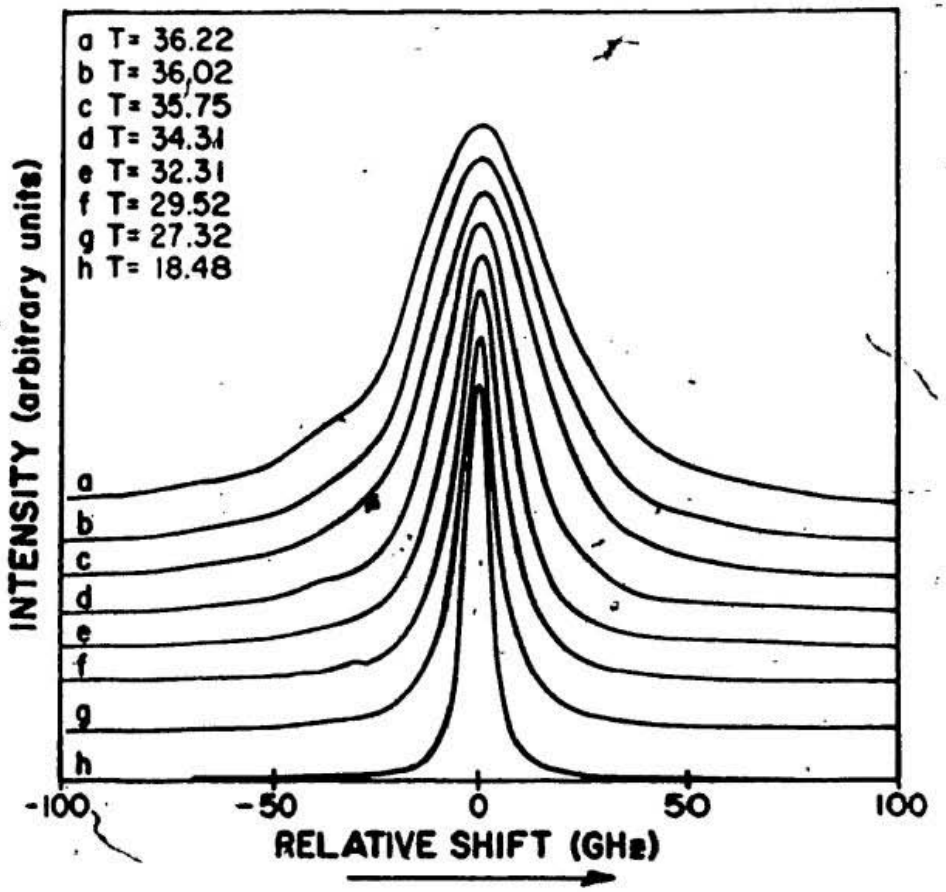

FIG. 11e. The Q-branch of liquid HD along the vapor-liquid coexistence curve (SFR=215 GHz for a-e, and SFR=117 GHz for f-h).

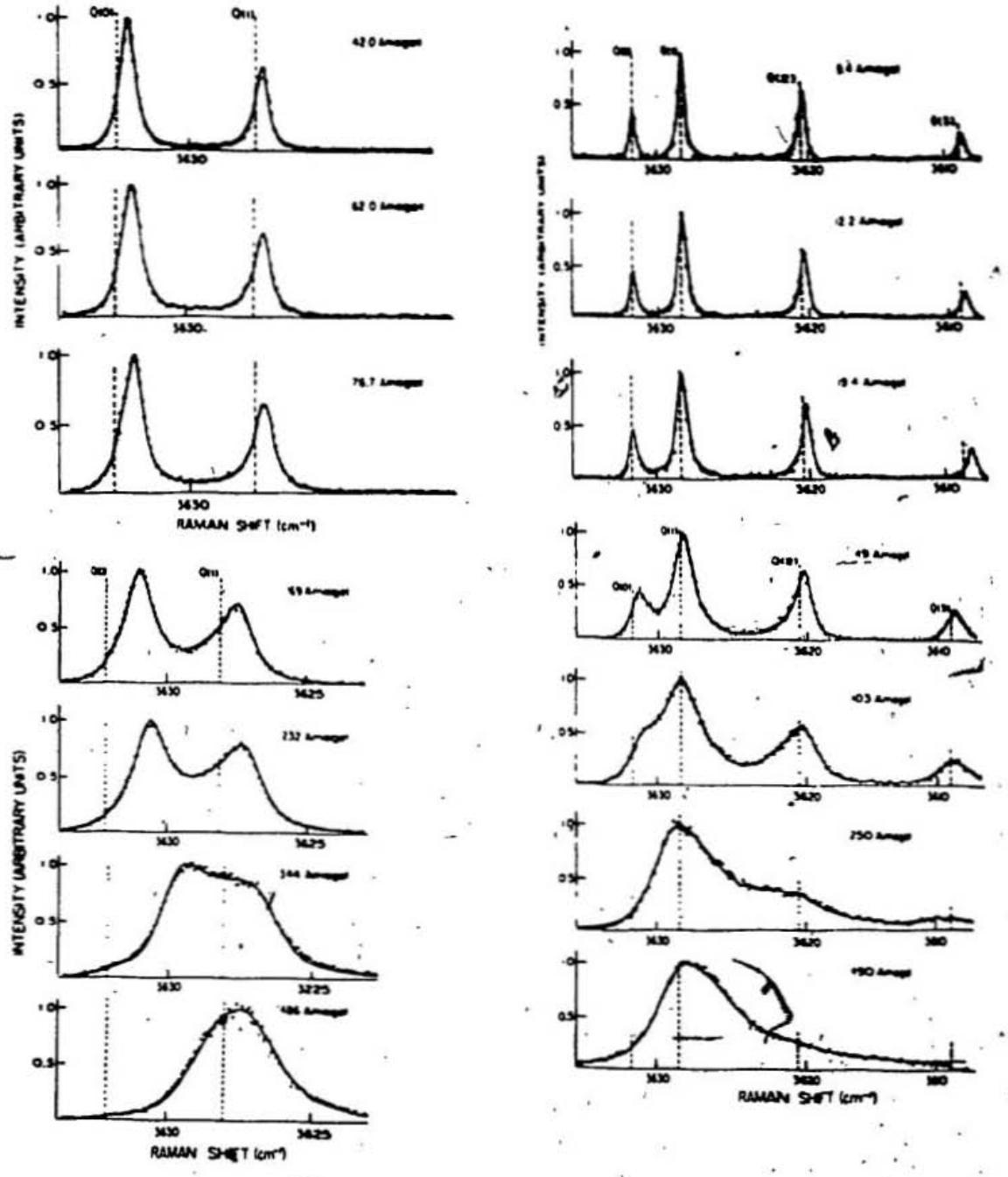

FIG. 12. The Q-branch of HD for different densities at 85 K, (left side of figure) and room temperature (right side) (Ref. 7).

difference beeing that the Q(1) feature is much weaker.

The spectra of Fig. 12 also demonstrate the collapse of the entire Q branch into a single component as the density is increased above about 300 amagat. This marks the onset of a particular spectral narrowing process which arises from the indirect dephasing of the vibrational motion via vibration-rotation coupling. This phenomenon has been discussed in Chapter II and to a first approximation is to be regarded as distinct from the direct, or pure, dephasing process considered by Hills and Madden (for example). It has been the focus of attention in several publications[3,7,11] on HD, and is reasonably well understood. In the present case it is a matter of coincidence that the critical density of HD (357 amagat) is sufficiently high for the effect to warrent consideration. There is, for example, little doubt that the effect is responsible for the absence of the Q(1) transition as a separate component in spectra recorded on the critical isochore. In Fig. 11a the only indication of its presence is in the asymmetry of the 55.28 K profile where its intensity is enhanced by the relatively high temperature. It is also appropriate to note that in this (critical isochore) case the circumstances which give rise to the collapse of the Q(0) and Q(1) features into a single component are unique. Normally[7] the process occurs with increasing density as pressure-broadening causes the individual features to overlap (see Fig. 12). From the behaviour of the spectra in Fig. 11a (as discussed below) it is apparent that the broadening of the individual features is primarily a critical effect which occurs at constant density as the temperature approaches T_C. The situation is complicated, however, by the

rapid weakening of the Q(1) component with decreasing temperature, and it is debatable whether this particular mechanism has any significant effect on the spectral profile near T_C.

For the higher isochoric density of 803 amagat (Fig. 11b) there is no evidence of the Q(1) feature, and the spectrum is considerably narrower, as expected. On the lower density isochore at 180 amagat (Fig. 11c) a weak Q(1) component is evident at the higher temperatures where its visibility is enhanced by its smaller width (since the normal pressure-broadening mechanism is less effective at low densities). In these latter spectra the measured ($\approx$75 GHz) separation of the two components is in agreement with the results of Witkowicz and May[7].

It should be noted that most of the spectra were obtained using a SFR of 215 GHz and the Q(1) component, where visible, occurs (e.g. spectrum n, Fig. 11a) in the same Fabry-Perot interference order as Q(0). In these cases the relative positions of the two components are correctly represented, with the Q(1) component on the low-shift side of Q(0). In cases where a smaller SFR of 117 GHz was required to resolve the spectrum the Q(1) component, where visible, is shown in an adjacent interference order and is not in its correct relative position (see Fig. 11c). Fortunately because of the weakness of the Q(1) feature, this situation (which was largely unavoidable) did not seriously affect the analysis which is described in the following sections. Attention will be drawn to cases where the effect is believed to be significant.

In comparing the various profiles (Figs. 11a-e) the zero of intensity for each spectrum is successively incremented to permit stacking. Also, any variation of peak frequency with temperature or density has, for reasons of clarity, been neglected. These (lineshift) effects are discussed in a separate section below.

2. SPECTRAL ASYMMETRY

The asymmetry of each spectrum was measured as a simple ratio of the half-widths at half-maximum (HWHM) which were taken to be intrinsically positive. In Fig. 13 this measure is given as HWHM[HI]/HWHM[LO], where the [HI] designation refers to higher Raman shifts and [LO] refers to lower Raman shifts: for convenience it will be referred to as the **asymmetry factor**, AF. Values of AF$\approx$1 indicate a high degree of symmetry, and it will be noted that values which are significantly <1 or >1 occur.

On the critical isochore (Fig. 13a), for example, AF rises sharply to a maximum value of about 1.3 as the critical point is approached. This is characteristic of the critical effect which has been observed in other systems[20], and the sense of the asymmetry (AF$>$1) is opposite to that which one might expect from the presence of a weak Q(1) line. This observed behaviour of AF therefore indicates that the Q(1) feature is sufficiently weak so that the associated modification of the near-critical profile may perhaps be neglected. At higher ($>$40 K) temperatures the AF values tend to be less than unity, and this reversal of the asymmetry is consistent with the emergence of the Q(1) transition as a separate feature (see spectrum n of Fig. 11a).

The corresponding plot for the low density isochore ($0.504\rho_C$) is shown in Fig. 13b. In this case the choice of SFR=117 GHz represents a compromise where the resolution is less than optimum but serious overlap of the two Q lines is avoided. As a result the values of AF are less accurately determined. At

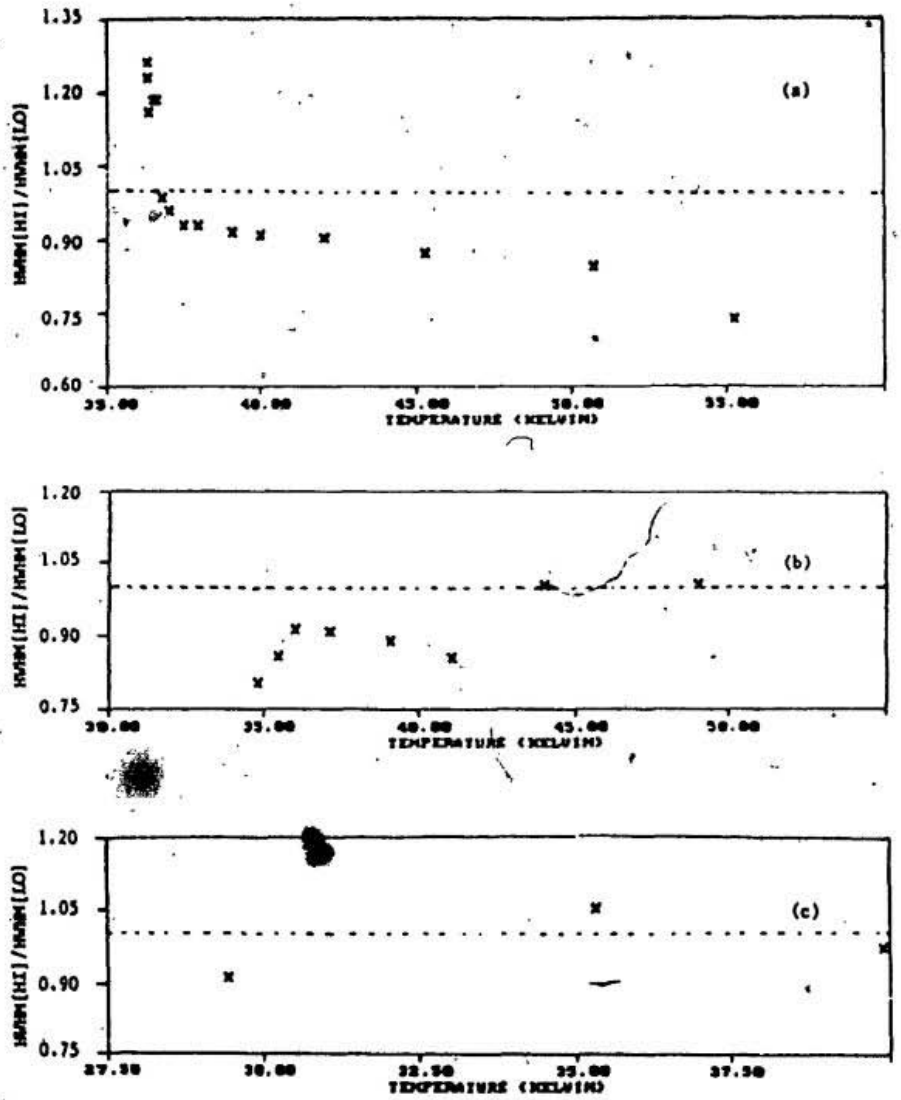

FIG. 13. Temperature and density dependence of the spectrum asymmetry :

(a) along critical isochore $\rho = \rho_C = 357$ amagat,

(b) along isochore $\rho = 0.504\ \rho_C$,

(c) along isochore $\rho = 2.25\ \rho_C$,

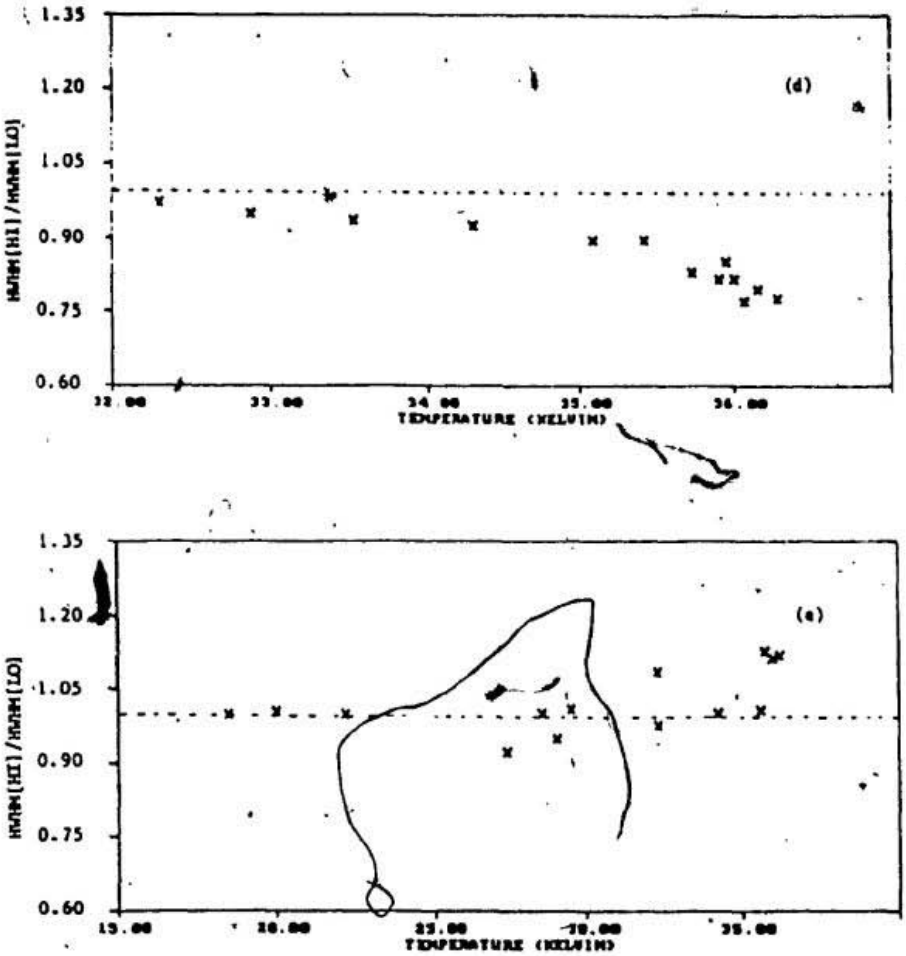

FIG. 13. Temperature and density dependence of the spectrum asymmetry :

(d) in vapor along vapor-liquid coexistence curve,

(e) in liquid along vapor-liquid coexistence curve,

The asymmetry was measured as a ratio of half-widths at half-maximum (HWHM) corresponding to the high-shift side [HI] and the low-shift side [LO] of each profile.

temperatures below about 40 K (i.e. closer to T_C), where the Q(1) component was not detected, AF is less than unity as in the near-critical vapor (see below). As pointed out above, the Q(1) feature becomes visible at the higher temperatures and occurs in an adjacent interference order on the high-shift side of Q(0). It has the extraneous effect of nullifying the lower temperature asymmetry.

For the high density ($2.25\rho_C$) isochore of Fig. 13c the same SFR (117 GHz) was used for the same reasons. It turned out, however, that the Q(1) component was nowhere visible as a distinct feature because of the collapse and narrowing of the entire spectrum with increased density (see Fig. 11c). These profiles were highly symmetrical and only three spectra were recorded because of the relative insensitivity to temperature.

The behaviour of the vapor spectra (Fig. 13d) is similar to that for the low density isochore (Fig. 13b) in that AF$<$1 and decreases as the critical point is approached. The difference here, of course, is that the density increases from $0.28\rho_C$ to $\approx\rho_C$ over the temperature range of Fig. 13d, and the spectral width approaches the maximum values observed on the critical isochore. It was for this reason that the SFR was chosen to be 215 GHz as in the latter case. There was little evidence of the Q(1) component in these spectra, and it is reasonable to assume that it can be neglected. The asymmetry is opposite in sense to that observed on the critical isochore but the same (in sense) as that for the low density isochore near T_C. This behaviour is, again, consistent with results[20] for N_2 and appears to be characteristic of the critical effect.

Most of the liquid-phase spectra were also recorded with SFR=215 GHz because near T_c the width increased to essentially the same values as for corresponding spectra on the critical isochore and in the vapor. Only the lowest temperature (highest density) spectrum of Fig. 11e was sufficiently narrow to require SFR=117 GHz. Again, there was no evidence of the Q(1) component and the spectra were for the most part highly symmetric. There was some evidence for AF>1 near critical point.

3. LINESHIFT

The theory of the density dependence of the vibrational Raman shifts in H_2 was first proposed by May and coworkers[56,57], and further developed by Gray and Van Kranendonk[58]. The effect is associated with perturbations of the vibrational motion by isotropic intermolecular forces for which the Lennard-Jones potential provides an adequate description. The theory predicts that the Q-branch Raman shifts can be expressed as an expansion in powers of the density :

$$\Delta Q = Q - Q_o = a_J \rho + b_J \rho^2 + \cdots , \qquad (3\text{-}1)$$

where Q represents the shift at density ρ, and Q_o is the shift for $\rho \to 0$. The coefficients a_J and b_J depend on the (lower state) rotational quantum number, J, and also on the temperature. At temperatures below about 300 K the a_J values are expected to be (increasingly) negative as a reflection of the more important role played by the attractive intermolecular forces. In assuming this theory to be generally valid for the hydrogens, it was noted[56] that the a_J and b_J values were predicted to be the same for both H_2 and HD. The results of Witkowicz and May[7] showed this to be approximately true, but there were other points of detail which cast doubt upon this assumed generality. It was consequently concluded[7] that further theoretical work was required in this connection.

TABLE I. The temperature dependence the a_0 and b_0 coefficients for HD.

TEMP. K	a_0 GHz/amagat	$b_0 \times 10^4$ GHz/amagat^2
293[a]	-0.034±0.002	1.62±0.78
85[a]	-0.165±0.042	0
<35.10[b]	-0.27±0.02	0

a - Ref. 7, b - present studies.

In the present case the results which are most appropriate for comparison with the above work are for non-critical liquid and vapor corresponding to the regions below about 35 K in Figs 14d and e. These results are, of course, also subject to the influence of varying temperature. However, the isochoric plots of Figs. 14b and c show this effect to be of order 5% as compared to the overall liquid and vapor shifts, and for the present purposes it will be neglected. In accordance with Eq. (3-1) the data are plotted as a function of ρ in Fig. 15. The liquid data exhibit a distinct break between two linear regions corresponding (i) to the low-density, near-critical regime and (ii) to the high-density, non-critical conditions which are of interest in this particular comparison. A similar though less distinct behaviour is also observed for the vapor, and in this case attention should be focussed on the lowest densities where the slope is comparable to that

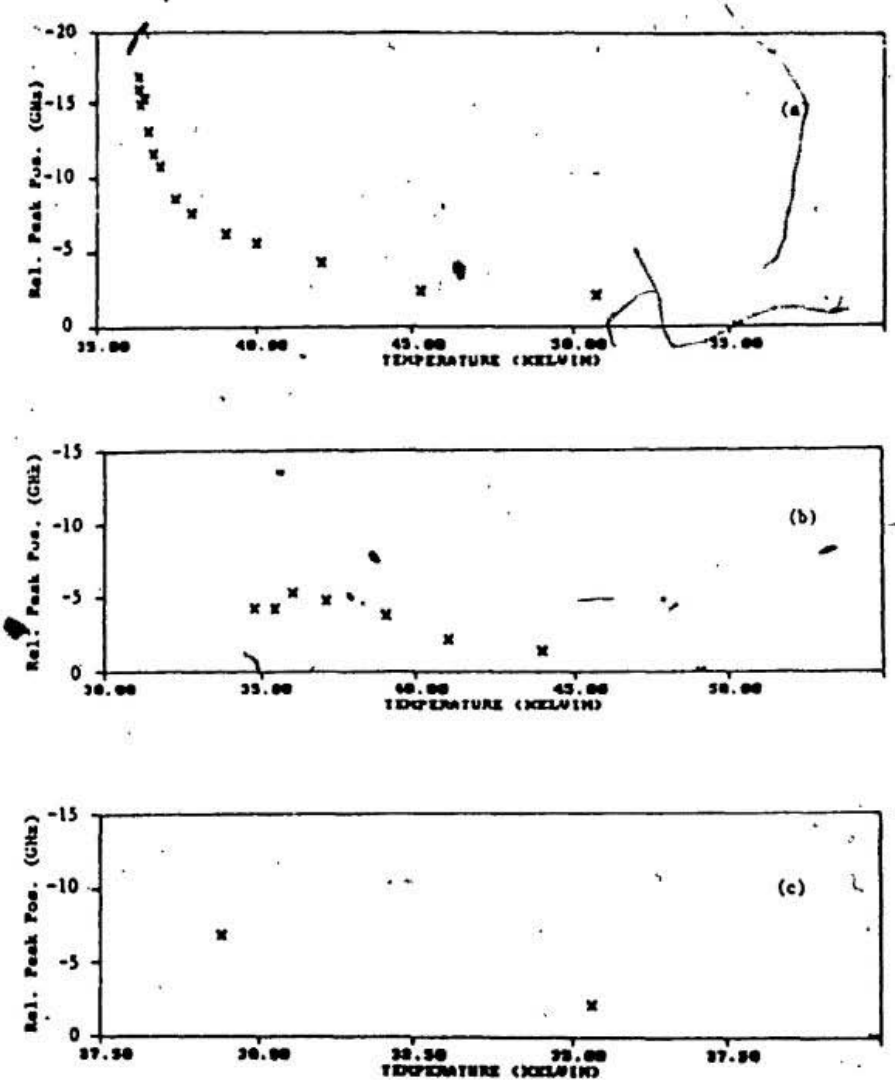

FIG. 14. Temperature and density dependence of the Q(0) peak position :

(a) along critical isochore $\rho = \rho_C = 357$ amagat,

(b) along isochore $\rho = 0.504\ \rho_C$,

(c) along isochore $\rho = 2.25\ \rho_C$,

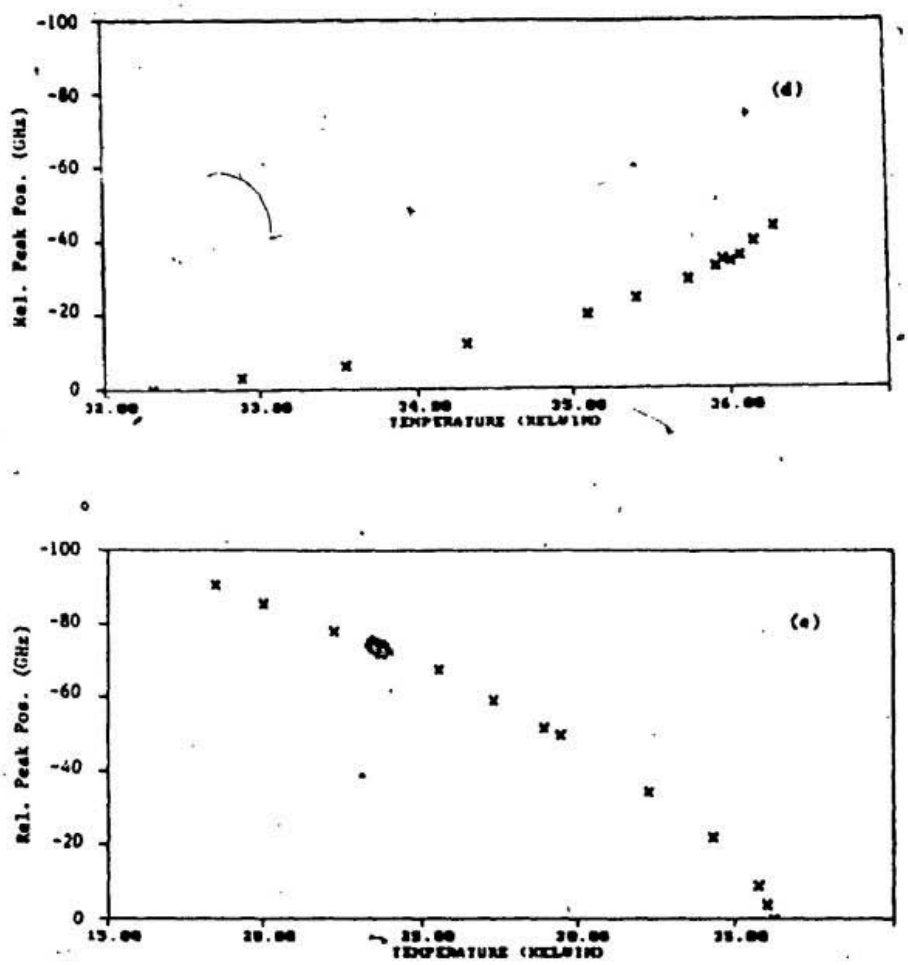

FIG. 14. Temperature and density dependence of the Q(0) peak position :

(d) in vapor along the vapor-liquid coexistence curve,

(e) in liquid along the vapor-liquid coexistence curve,

In each case the relative position of 0 GHz is assigned to the highest value of the Raman shift (i.e. the ordinate values mean decreasing shift).

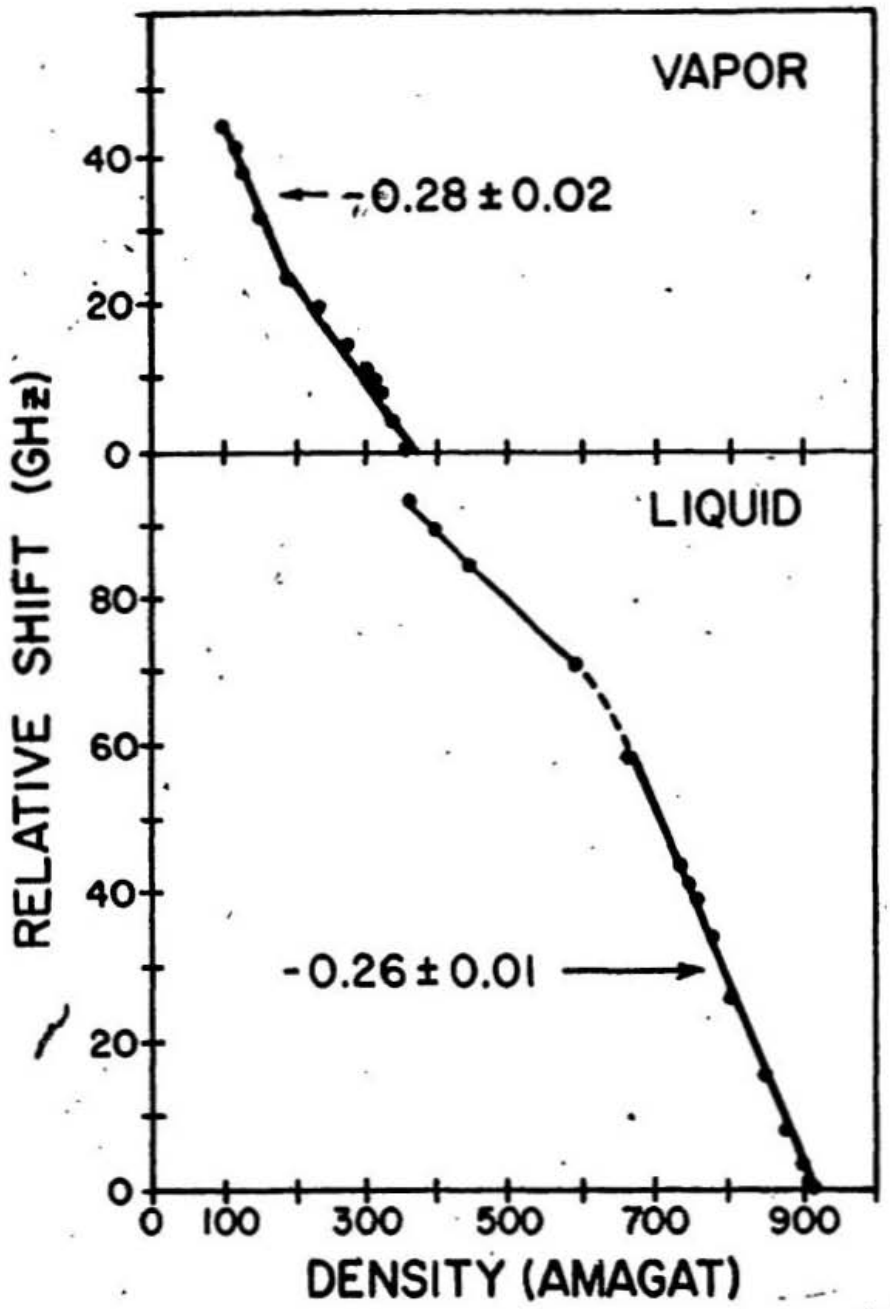

FIG. 15. Plot of the relative Raman shifts versus density for HD vapor (upper part of figure), and liquid (lower), along the vapor-liquid coexistence curve. The calculated slopes are shown.

region (ii). From the average of these slopes, and recognizing that Q(0) was the only component present in both cases, it is concluded that a_0=-0.27 GHz amagat^{-1} and b_0=0. These values are included in Table I, which demonstrates a consistency with the data of Witkowicz and May in two respects. First, b_0=0 as for their lower temperature results and, second, the magnitude of a_0 exhibits an obvious trend to higher values with decreasing T. The latter behaviour is not unexpected, given the increased dominance of attractive forces at lower temperatures, but beyond this, little further comment can be made.

The behaviour of the remaining data in Fig. 15 is most probably determined by critical effects. The possible contribution of Q-branch collapse can be readily estimated because its maximum effect is to displace the Q(0) peak position to the centre of gravity of the branch. Since the Q(1) component has a relative intensity of only 4%, the maximum contribution is of order $0.04 \times 75 \approx 3$ GHz, and this is small compared to the $\approx$20 GHz change in peak position which occurs through the non-critical region in each of the liquid and vapor cases. Furthermore, the effect should be such as to enhance the normal density dependence of the shift (see Fig. 12), whereas the converse is observed. On the other hand, above 20 GHz the change is about 1/3 of the full-width at half-maximum (discussed in the next section) at the critical point, so that deviations of the slope from -0.27 GHz amagat^{-1} could quite conceivably result from rather subtle changes in the shape of the profile which accompany the critical broadening. This is also borne out by the behaviour on the critical isochore (Fig. 14a) where the normal density

dependence of the shift is absent. In this case the change in peak position through the near-critical region (where the sharp increase occurs) is about 10 GHz. Given a maximum contribution of ≈3 GHz from other sources, it is concluded (consistent with the discussion of spectral asymmetry above) that the primary effect is associated with the critical phenomenon.

Further to the last comment, there is also a minor contribution to the shift variation on the critical isochore arising from the normal temperature dependence of a_0. This is more clearly demonstrated in the constant-density ($0.504\rho_C$, $2.25\rho_C$) plots of Figs. 14b and c where critical effects can be neglected. In both cases the peak position changes at a rate of about +0.35 GHz K^{-1} which is negligible compared to the near-critical slope in Fig. 14a. It is noted in passing that the pure temperature dependence of the shift has the appropriate sign to be consistent with the idea that the dominance of the attractive forces is eroded with increasing temperature.

4. LINEWIDTH

On the basis of the foregoing, the mechanism of Q-branch collapse, and its particular contribution to the (motional) narrowing of the spectrum at high densities, will be regarded as negligible. It will be excluded from consideration in the linewidth discussion. The contribution to the spectral width arising from the finite lifetime of the v=1 state (i.e. energy relaxation) can also be quite safely neglected because the inverse of the known[59] (30 ms) lifetime for H_2 is 9 orders of magnitude less than the presently observed widths. The effect of resonant transfer of the v=1 excitation between molecules can be assessed by isotopic dilution of the active species. This was effectively done in the present case via the spectra of the H_2 and D_2 impurities. These spectra were very weak (at concentration of ≈3%), but it was nevertheless clear that the effect can as a first approximation be neglected. It is appropriately regarded as a matter of detail which warrents further investigations in the future.

Apart from critical effects, this leaves only two identifiable mechanisms for consideration, namely, **pressure broadening** and **pure dephasing**. The first of these is responsible for the behaviour at low densities, where the individual Q branch components are observed to broaden with increasing density (see Fig. 12), while the second can be expected to cause the reverse effect of narrowing at high densities. This behaviour is in fact demonstrated by a comparison of Figs. 16b and c where the densities differ by a factor of ≈5 and yet the widths are essentially the same. This is also consistent with the behaviour of the liquid and vapor

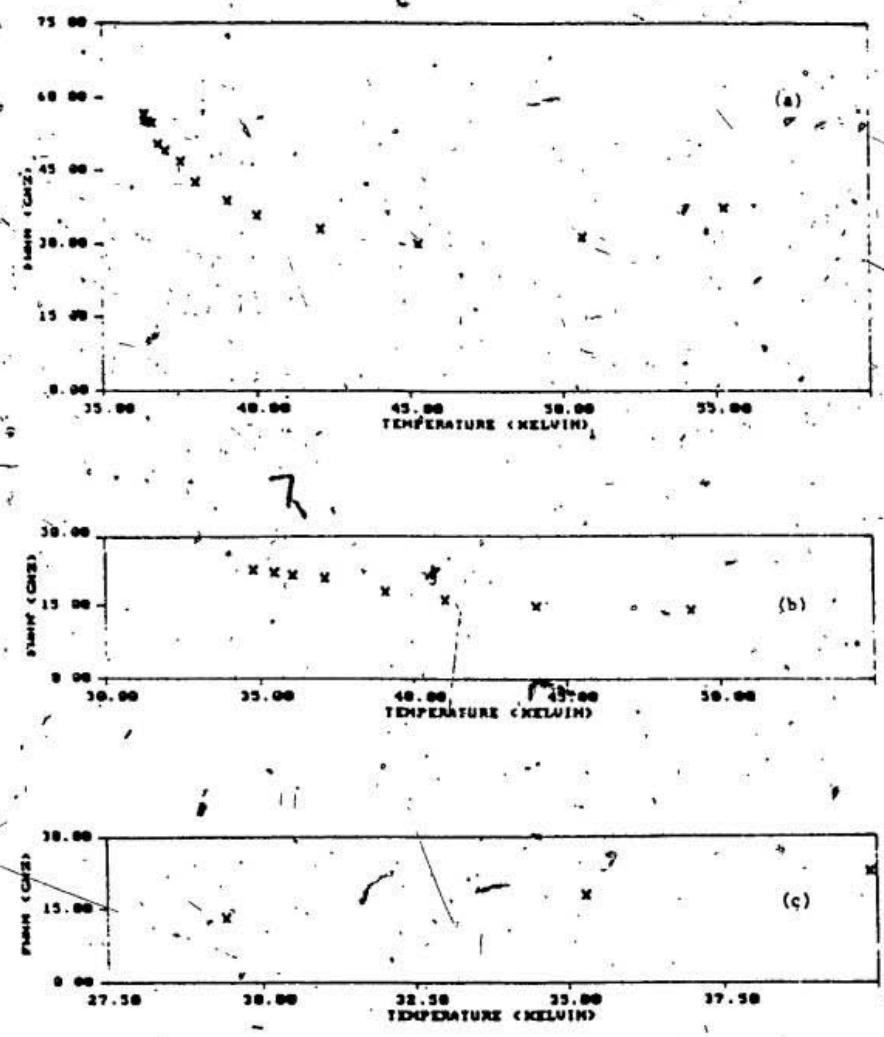

FIG. 16. Temperature dependence of the FWHM for Q(0) measured:

(a) along critical isochore $\rho = \rho_C = 357$ amagat,

(b) along isochore $\rho = 0.504\ \rho_C$,

(c) along isochore $\rho = 2.25\ \rho_C$.

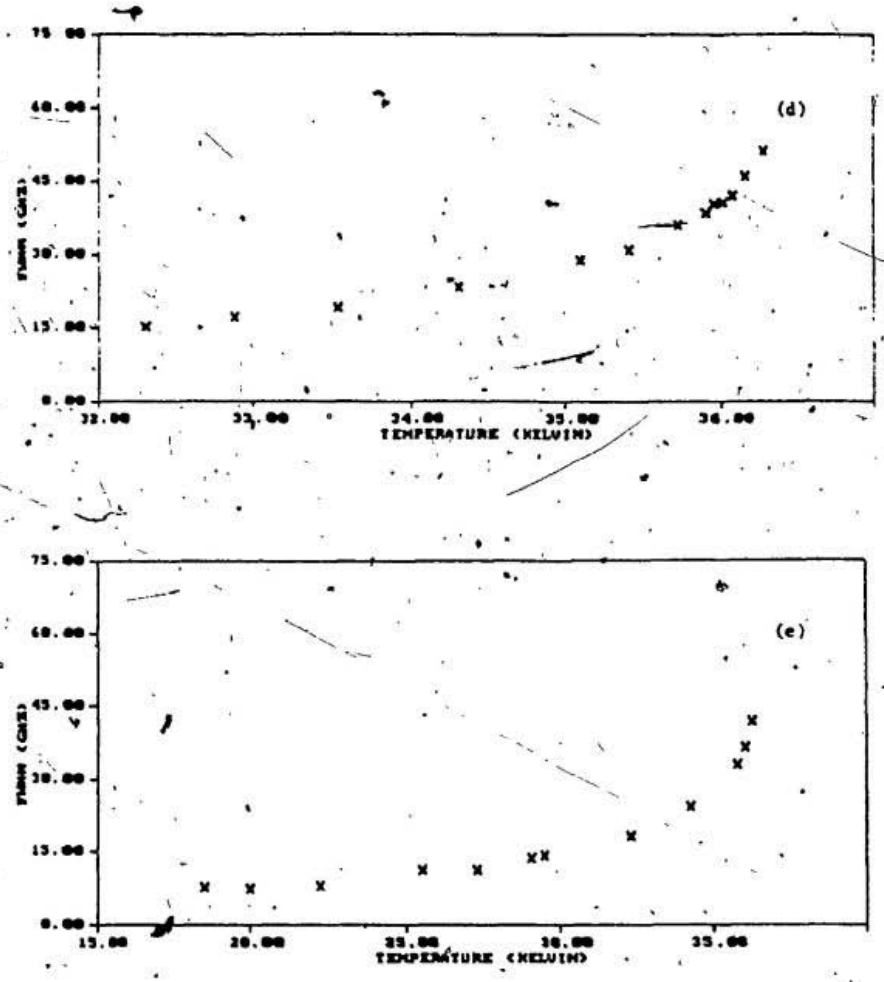

FIG. 16. Temperature dependence of the FWHM for Q(0) measured :

(d) in vapor along vapor-liquid coexistence curve,

(e) in liquid along vapor-liquid coexistence curve,

(Figs. 16d and e). It is thus apparent that the maximum width arising from the interplay of these two mechanisms occurs at densities comparable to ρ_C, but the details of the normal behaviour are obscured by the more dramatic critical effects (Figs. 16d and e). This is further supported by a closer examination of the non-critical data and the associated theory.

The theory of pressure broadening has been treated in considerable detail by Van Kranendonk and coworkers[9,58]. They have shown that for the Raman Q branch the principal effect is associated with rotationally inelastic collisions which limit the lifetime of states corresponding to different J. The low density results of Witkowicz and May[7] confirm the linear density dependence of the broadening as well as the dependence of the broadening coefficient (B) on temperature. For example, their B values for the Q(0) line at 293 K and 85 K were quoted as 0.86 GHz amagat^{-1} and 0.15 GHz amagat^{-1}, respectively. While no direct determination of B was made in the present experiments an estimate can be obtained by the comparison of non-critical widths at the densities of ρ_C and $0.504\rho_C$ (Figs. 16a and b). The value of 0.08 GHz amagat^{-1} obtained at T$\approx$45 K is undoubtedly an overestimate because of additional (critical) broadening effects at the higher density. It is nevertheless consistent with the expected trend, and a corresponding estimate obtained from the low-density vapor (Fig. 16d) is in agreement. The slight increase in width which occurs with decreasing temperature in Fig. 16b appears to be in contradiction. However, as noted[20] in the case of N_2 and in the discussion of spectral asymmetry above, an effect of this magnitude could easily

be associated with a residual critical broadening which appears to persist on this lower density isochore.

With respect to the data on the high density isochore (Fig. 16c), the linear decrease in width at a rate of about 0.9 GHz K^{-1} may be significant. This is consistent with theory which predicts[60] that the dephasing linewidth in the motional narrowing limit should be proportional to the T^2/D_s where D_s, the coefficient of self diffusion, can be assumed proportional to T at temperatures not too close to a phase transition point. The non-critical liquid data of Fig. 17 also appear to confirm the expected[10] ρ^{-1} dependence of the linewidth at high densities. However, the combination of these two dependences suggests a liquid linewidth at 18 K which is considerably less than the 7 GHz value actually observed (Fig. 16e). This may result from a more rapid decrease of D_s with temperature as the triple point (16.60 K) is approached.

The behaviour on the critical isochore (Fig. 16a) is again dominated by critical broadening which gives rise to a 2-fold increase in width. The slight increase in width at the highest temperatures is due to the emergence of the Q(1) component (see Fig. 11a) whose main effect is to increase the asymmetry ($AF<1$) of the Q(0) profile (Fig. 13a).

The liquid data of Fig. 16e offer an opportunity for comparison with theory of Hills and Madden[42] (see Chapter III) because (i) it follows from previous considerations that the behaviour is dominated by the pure dephasing mechanism, and (ii) the lineshape, to be discussed below, was determined to be Lorentzian so

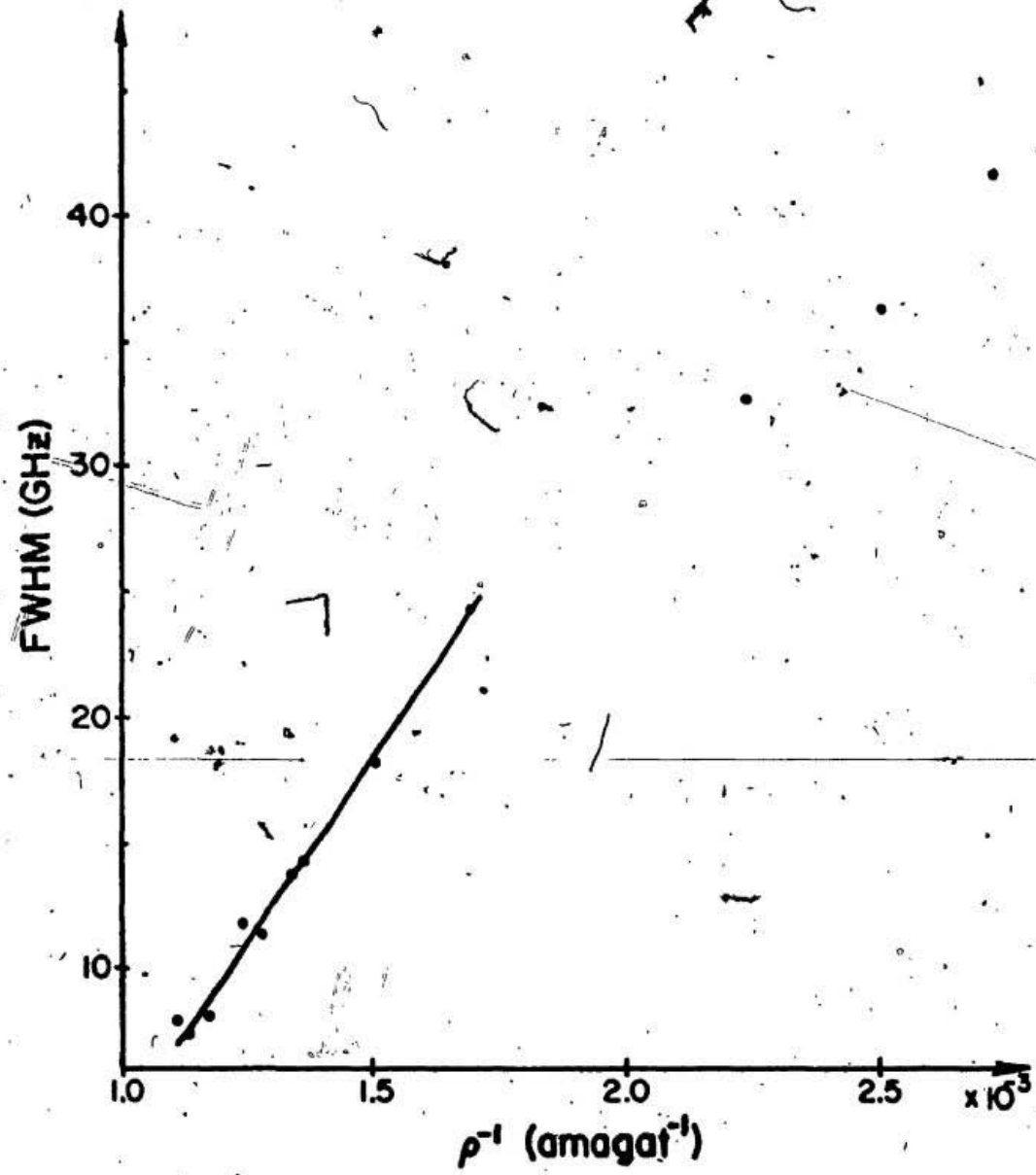

FIG. 17. Plot of the Full-Width at Half-Maximum (FWHM) of liquid HD Q(0) line along the liquid-vapor coexistence curve versus inverse density.

that fast-modulation conditions can be assumed to apply. Fig. 18 shows the appropriate plot for this purpose, where the symbol Γ now stands for FWHM. Two linear segments are apparent: nearest the critical point (where $\Gamma >> \phi$) the slope is λ_{2EXP}=-0.09, while furthest from the critical point (where $\Gamma << \phi$) it is λ_{1EXP}=-0.43. Using published values for the critical exponents[61-65], the simplest hydrodynamic approximation[42] predicts

$$-1.57 < \lambda_{1CALC} < -1.13, \qquad (4\text{-}1)$$

$$-0.56 < \lambda_{2CALC} < -0.16, \qquad (4\text{-}2)$$

or by using the Kawasaki correction[66]

$$-0.22 < \lambda_{2KCALC} < 0.16 \qquad (4\text{-}3)$$

(Note that λ_1 is not affected by the Kawasaki correction). Thus the observed value, λ_{2EXP}, and calculated values λ_{2KCALC}, are in approximate agreement, while such is not the case for λ_1. This is in agreement with the corresponding analysis[17] of data for liquids N_2, O_2, and CH_4, and leaves little doubt that Hills and Madden approach is not appropriate for large ϵ. The reason is presumably that the use of critical exponents is not justified in this region.

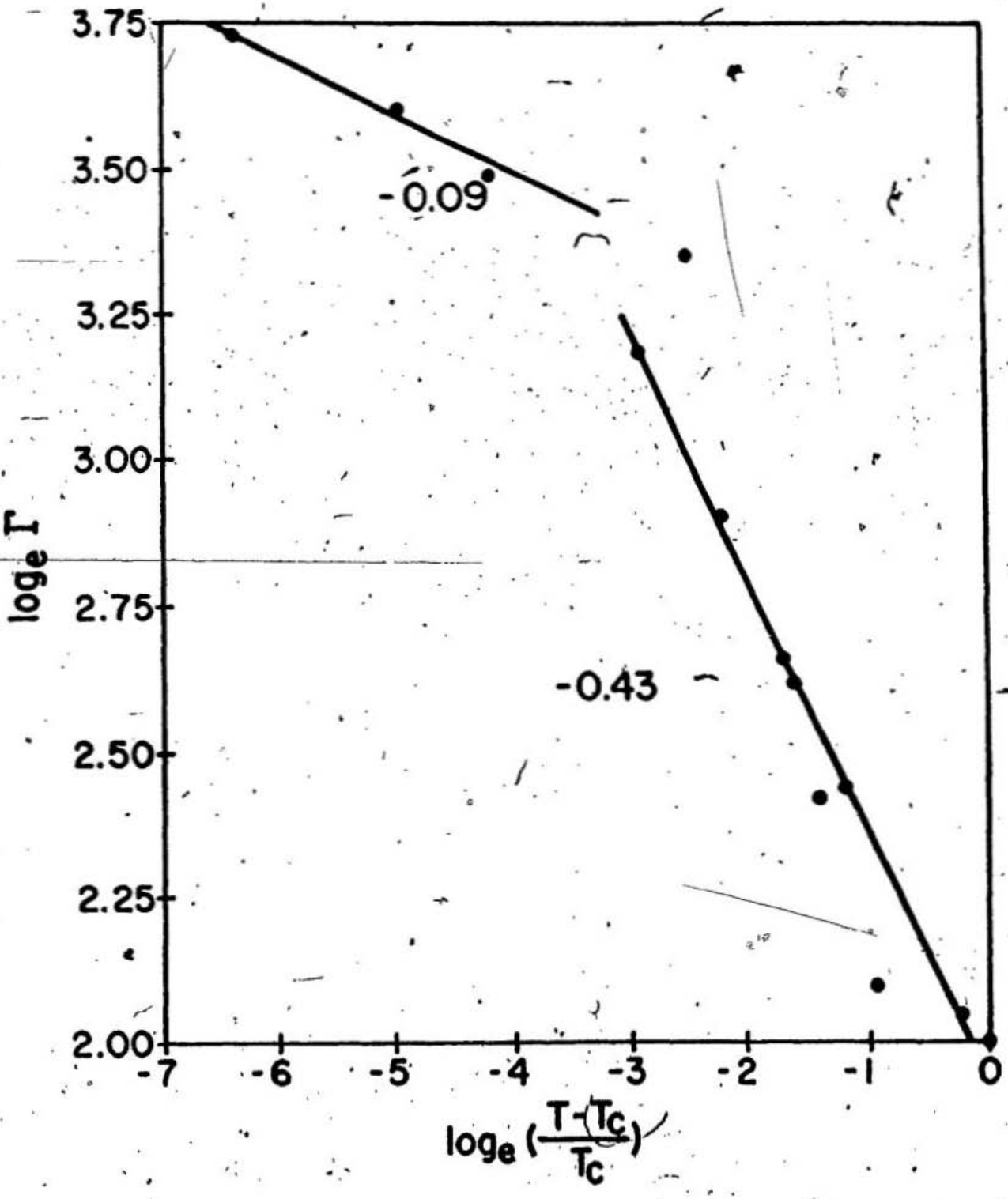

FIG. 18. Logarithm of the linewidth (FWHM) versus the logarithm of the reduced temperature (ϵ) for HD. Slopes of lines are indicated.

5. LINESHAPE ANALYSIS

The Gaussian versus Lorentzian character of the profiles was determined from a least-squares fit of Eq. (3-6) to the cosine transform of each spectrum, with the ratio of the v_2 (Gaussian) and v_1 (Lorentzian) parameters being used as a characteristic measure. The v_2/v_1 values obtained are plotted in Fig. 19 and clearly show that the Q(0) profile is accurately Lorentzian in shape under all conditions except for the smallest ϵ values on the critical isochore. As discussed above, the latter spectra were also distinctly asymmetric so that the Voigt profile alone can not be expected to accurately describe them.

Attempts were consequently made to analyse these spectra by the semi-empirical approach previously applied for N_2[20] and H_2[25]. The basis of the approach is that the dominant Gaussian characteristic for $\epsilon \to 0$ signifies the onset of the slow-motion condition which is expected[21,22] to obtain in this region. In other words, the long-lived spatial fluctuations in local density associated with the hydrodynamic modes gives rise to an inhomogeneous broadening in excess of the normal homogeneous width due to the high frequency motions. Under these conditions it is reasonable to model the spectrum as a superposition of local (Lorentzian) spectra whose characteristics are determined by the observed non-critical behaviour. The model is represented symbolically by the relation

$$I(\nu) = \int_0^{\rho_m} \rho\, L(\nu,\rho)\, P(\rho)\, d\rho \ , \qquad (5\text{-}1)$$

where $I(\nu)$ is the observed spectrum, ν is the shift relative to the peak of the

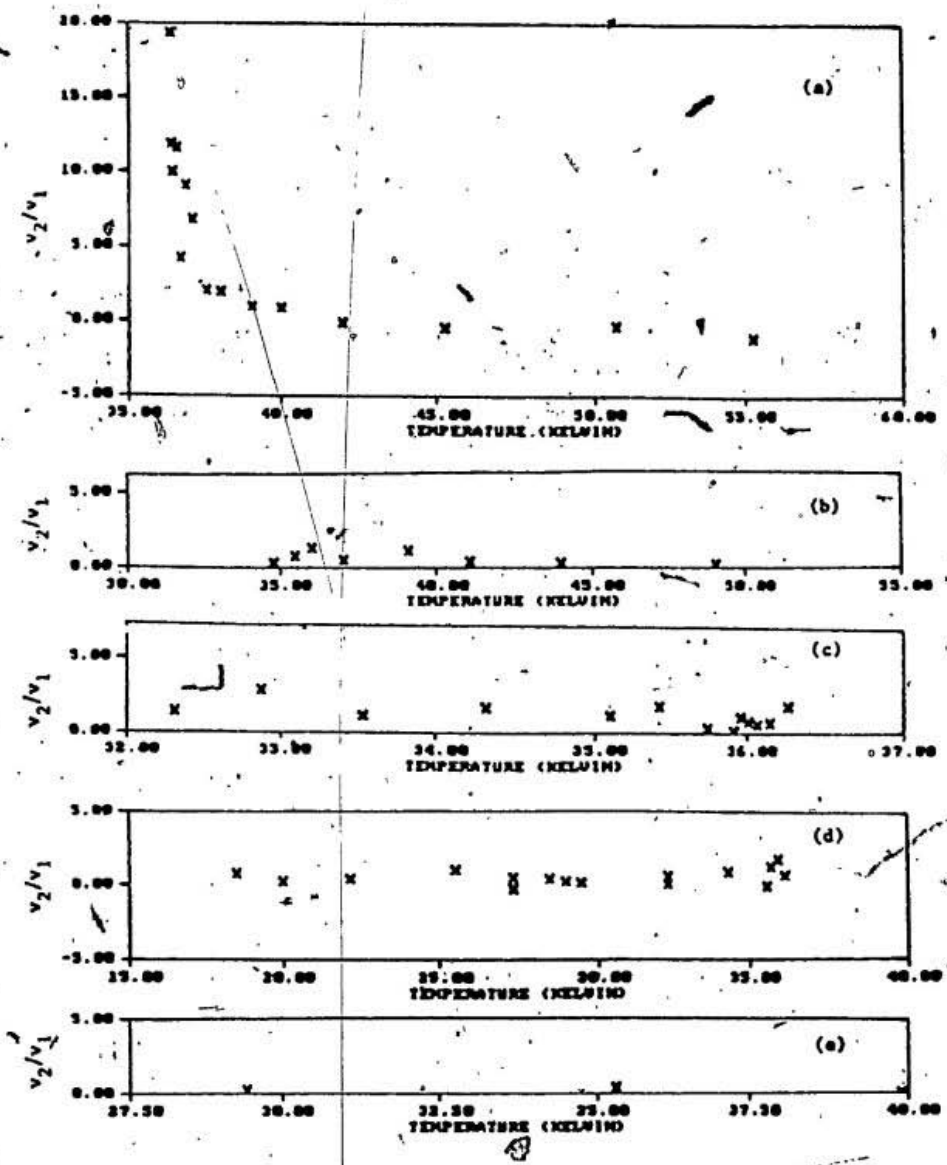

FIG. 19. Temperature dependence of the relative importance of the Gaussian versus Lorentzian content as measured by the ratio v_2/v_1 from Eq. (3-6) :

(a) along critical isochore $\rho = \rho_C = .357$ amagat,

(b) along isochore $\rho = 0.504\ \rho_C$,

(c) in vapor along vapor-liquid coexistence curve,

(d) in liquid along vapor-liquid coexistence curve,

(e) along isochore $\rho = 2.25\ \rho_C$.

profile, and ρ is the local density with ρ_m taken as a reasonable upper limit corresponding to the triple point value. $L(\nu,\rho)$ is a Lorentzian function of unit area

$$L(\nu,\rho) = \frac{2}{\pi\Gamma}\left[1+\left[2\frac{\nu-\nu_p}{\Gamma}\right]^2\right]^{-1}, \qquad (5\text{-}2)$$

This function models the local spectrum with a peak frequency, ν_p, and FWHM=Γ which depend on ρ in accordance with the non-critical behaviour. The intensity of each local spectrum is determined by the Gaussian weighting function, $P(\rho)$,

$$P(\rho) = (\sigma\sqrt{2\pi})^{-1}\exp\left[-\frac{(\rho-\bar{\rho})^2}{2\sigma^2}\right], \qquad (5\text{-}3)$$

which is the first approximation to the probability distribution for different local densities. The additional ρ factor occurs in the integrand of Eq. (5-1) for the obvious reason that the intensity of each local spectrum is also proportional to the local density. The only free parameter in this model is σ, i.e. the square root of the second moment (=0.425xFWHM) of the Gaussian distribution, and it is consequently the quantity of interest which can be determined by the application of least-squares fitting techniques. This procedure was applied with considerable success for both N_2[20] and H_2[25], and revealed an exponential dependence (see Fig. 20) for $\sigma(\epsilon)$ which did not conform with the power-law behaviour predicted by conventional theory. Subsequent extensions of the theory[21,22], which include the effects of finite volume, appear to satisfactorily explain these results.

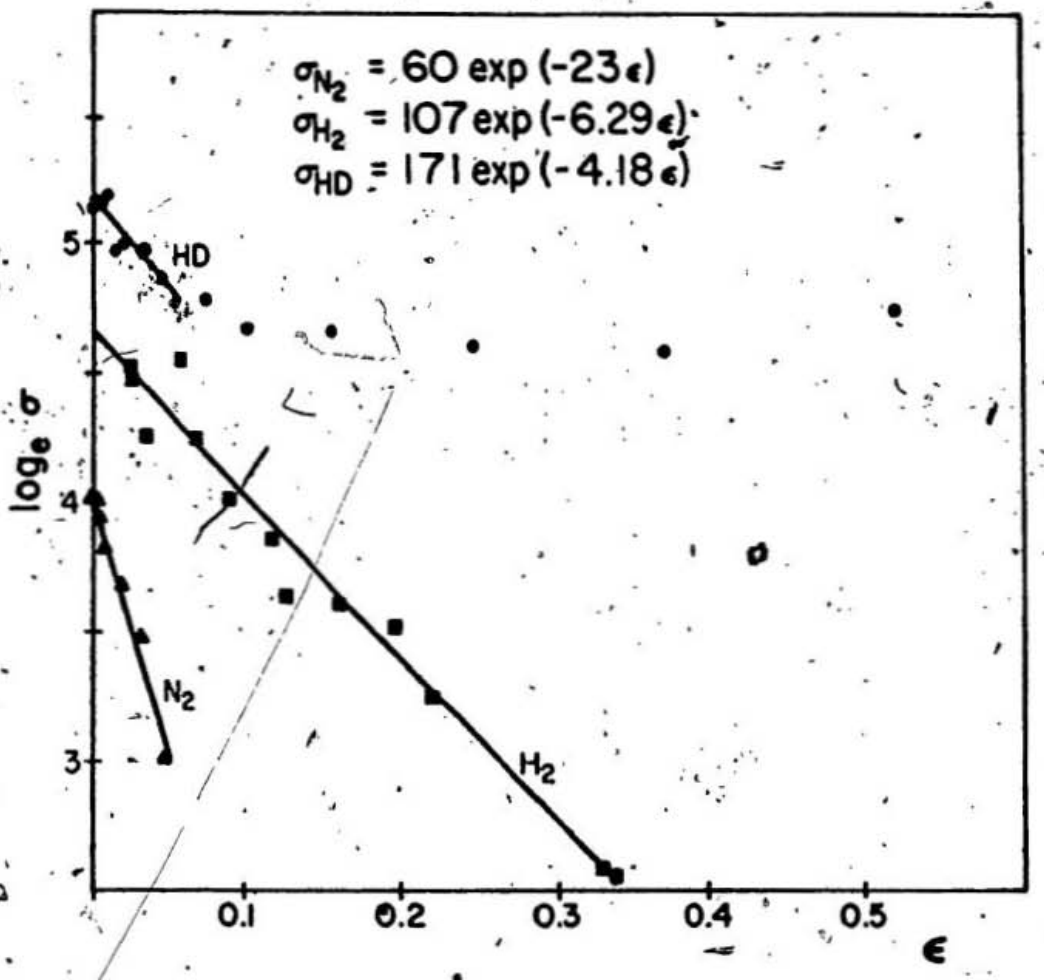

FIG. 20. Natural logarithm of the square root of the $P(\rho)$ second moment σ (in amagat units) versus ϵ on the critical isochores of N_2 (Ref. 20), H_2 (Ref. 25), and HD.

The analogous procedure was not successful for HD, apparently because of the presence of the weak Q(1) line. As noted in the discussion of asymmetry above, the effect of the Q(1) component becomes more significant as the temperature is raised along the critical isochore and, indeed, becomes an important factor in determining the shape of the spectral wing on the low-shift side. The consequences of this are apparent in Fig. 20 where the (possibly) linear region at small ϵ is not satisfactorially defined for HD, and the behaviour for large ϵ is in clear disagreement with that for N_2 and H_2. The straight line shown in Fig. 20 for HD was obtained by using the same $\Gamma(\rho)$ and $\nu_p(\rho)$ dependences as previously determined[25] for H_2, namely, Γ=constant= 10 GHz and $\nu_p = \nu_o - 0.147\rho$ (where ν_o is the free-molecule frequency for HD). Given the lack of success in applying this procedure, it was not considered worthwhile to persue the matter further. A more elaborate model which might attempt to account for the presence of the Q(1) component was not considered feasible because of the complications associated with the collapse of the Q branch occurring simultaneously with the critical broadening.

6. CONCLUSIONS

The behaviour of the Q(0) Raman spectrum of HD in the critical region is satisfactorily explained in terms of three mechanisms : (i) normal pressure broadening at low densities, (ii) pure vibrational dephasing at high densities, and, (iii) a specific kind of critical broadening which occurs in the immediate vicinity of the critical point. The special phenomenon of Q-branch collapse, which is in principle operative at densities near ρ_C, appears to contribute to the lineshape in matters of detail only. This is justifiable because only one other component of the branch, namely Q(1), was marginally observable with a relative intensity of $\approx$4%.

The critical broadening is consistent with corresponding effects observed in N_2 and H_2 where modelling of the lineshape revealed new information pertaining to the behaviour of the probability function for local density. In the case of HD this proved not to be feasible because of (otherwise negligible) distortion of the near-critical lineshape due to the presence of the weak Q(1) component.

The results suggest that future work in this region of the phase diagram should focus on those details of the behaviour which are determined by the normally active mechanisms identified as (i) and (ii) above. Each of these mechanisms can, in principle, be investigated independently by working at extremes of density where the complications of critical broadening are negligible. The information obtained could provide impetus for further theoretical work on a particularly simple fluid system where effectively all the molecules are in their ground

rotational and vibrational states.

REFERENCES:

1 Hara E.H., May A.D., and Knaap H.F.P., Can. J. Phys. 49, 420 (1971).

2 Hara E. H., and May A.D., Can. J. Phys. 50, 1227 (1972).

3 Dion P., and May A.D., Can. J. Phys. 51, 38 (1973).

4 Urey H.C., Brickwedde F.G., and Murphy G.M., Phys. Rev. 39, 164, (1932)

5 Farkas A., Orthohydrogen, parahydrogen, and heavy hydrogen, Cambridge Univ. Press, (1935).

6 Bhatnagar S.S., Allin E.J., and Welsh H.L., Can. J. Phys. 40, 9, (1962)

7 Witkowicz T., and May A.D., Can. J. Phys. 54, 575 (1976).

8 Bonamy J., Bonamy L., and Robert D., J. Chem. Phys. 67, 4441 (1977).

9 Fiutak J., and Van Kranendonk J., Can. J. Phys. 40, 1085 (1962).

Van Kranendonk J., Can. J. Phys. 41, 433 (1963).

10 Alekseyev V.A., Grasiuk A., Ragulsky V., Sobelman I., and Faizulov F., IEEE J. Quantum Electron. 4, 654 (1968).

Alekseyev V.A., and Sobelman I., Zh. Eksp. Teor. Fiz. 55, 1874 (1968). [Sov. Phys.-JETP 28, 991 (1969).]

Temkin S.I., and Burshtein, Pis'ma Zh. Eksp. Teor. Fiz. 24, 99 (1976). [JETP Lett. 24, 86 (1976)]; Chem. Phys. Lett. 66, 52 (1979); 66, 52 (1979); 66, 62 (1979).

11 Marsault-Herail F., Echargui M. Levi G., Marsault J.P., and Bonamy J., J. Chem. Phys. 77, 2715, (1982).

12 Rich N.H., and McKellar A.R.W., Can. J. Phys. 61, 1648 (1983)

McKellar A.R.W., and Rich. N.H., Can. J. Phys. 62, 1665 (1984)

McKellar A.R.W., Johns J.W.C., Majewski W., and Rich N.H., Can. J. Phys. 64, 227 (1986).

Clouter M.J., and McKellar A.R.W., Can. J. Phys. 65, 86 (1987).

13 Prasad R.D.G., and Reddy S.P., J.Chem. Phys., 62, 3582, (1975); 65, 83 (1976); 66, 707 (1977)

Reddy S.P. Induced Vibrational Absorption in the Hydrogens; from Phenomena Induced by Intermolecular Interactions, ed. G.Birnbaum (Plenum Publishing Corporation, 1985).

14 Jacobsen R.T.,and Stewart R.B., J. Phys. Chem. Ref. Data 2, 757 (1973).

15 Clouter M.J., and Kiefte H., J. Chem. Phys. 66, 1736 (1977).

16 Clouter M.J., Kiefte H., and Ali N., Phys. Rev. Lett. 40, 1170 (1978).

17 Clouter M.J., Kiefte H., and Jain R.K. J. Chem. Phys. 73, 673 (1980).

18 Deacon C.G., Clouter M.J., and Kiefte H., J. Chem. Phys. 83, 446, (1985).

19 Clouter M.J., and Kiefte H., Phys. Rev. Lett. 52, 763, (1984).

20 Clouter M.J., Kiefte H., and Deacon C.G., Phys. Rev. A 33, 2749 (1986).

21 Tuszynski J.A., Clouter M.J., and Kiefte H., Phys. Lett. 108A, 272, (1985).

22 Tuszynski J.A., Clouter M.J., and Kiefte H., Phys. Rev. 33B, 3423, (1986).

23 Landau L.D., and Lifshitz E.M., Statistical Physics, Pergamon Press, (1969).

24 Clouter M.J., Deacon C.G., and Kiefte H., Local Ordering in Fluid Deuterium, Phys. Rev. Lett. 58, 1116, (1987).

25 Deacon C.G., Clouter M.J., and Kiefte H., to be published.

26 Raman C.V., and Krishnan K.S., Indian J. Phys. 2, 387, (1928).

27 Smekal A., Die Naturwiss 11, 875, (1923).

28 Kramers H.A., and Heisenberg W., Z. Physik 31, 681, (1925).

29 Dirac P.A.M., Proc. Roy. Soc., (London), 114, 710, (1927).

30 Krishnan R.S., Historical Introduction, from book The Raman Effect, ed. Anderson A., Marcel Dekker, Inc., New York (1971).

31 Rothschild W.G., J. Chem. Phys. 65, 455 (1976).

Rothschild W.G., Dynamics of Molecular Liquids, J. Wiley & Sons (1984).

32 Baranska H., Labudzinska A., and Terpinski J., Laser Raman Spectrometry - Analytic Applications, (in Polish), PWN Warsaw (1981).

33 Herzberg G., Molecular Spectra and Molecular Structure, vol. 1 - Spectra of Diatomic Molecules, D. Van Nostrand (Canada) Ltd (1968).

34 Sakurai J.J., Advanced Quantum Mechanics, Addison-Wesley (1967).

35 Craig D.P., and Thirunanachandran T., Molecular Quantum Electrodynamics, Academic Press (1984).

36 Messiah A., Quantum Mechanics, North Holland Publishing Co., Amsterdam, The Netherlands (1962).

37 Rousseau D.L., Friedman J.M., and Williams R.F., The Resonance Raman Effect, from book: Raman Spectroscopy of gases and liquids, ed. Weber A., Topics in Current Physics vol.II, Springer Verlag (1979).

38 Placzek G., Z. Physik 70, 84 (1931).

39 Oxtoby D.W., Adv. Chem. Phys. (1978).

40 Knee L.B.G., The Vibrational Raman Effect: A Probe of The Molecular Environment, Bachelor of Science Thesis, Memorial University of Newfoundland, (1983)

41 Kubo R. Fluctuation, Relaxation and Resonance in Magnetic Systems, ed. Harr D.T., Oliver and Boyd, Edinburgh, (1961).

42 Hills B.P., and Madden P.A., Mol. Phys. 37, 937 (1979).

43 T. Andrews, Phil. Trans. R. Soc., 159, 575 (1869).

44 Fisher M.E., Scaling, Universality and Renormalization Group Theory, from book Critical Phenomena, Lecture Notes in Physics 186, ed. Hahne F.J.W., Springer-Verlag (1983).

45 Domb C., and Green M.S., Phase Transitions and Critical Phenomena. Academic Press (1976).

46 Hopkinson J., Proc. R. Soc., 48, 1 (1890).

47 Fetter A.L., Lectures on Correlation Functions, from book Critical Phenomena, Lecture Notes in Physics 186, ed. Hahne F.J.W., Springer-Verlag (1983).

48 Stanley H.E., Introduction to Phase Transitions and Critical Phenomena, Oxford University Press (1971).

49 Krynicki K, Powels J.G., and Rigamonti A., Mol. Phys. 34, (1977).

50 Gammon P. Master's Thesis, Memorial University of Newfoundland (1978)

51 Jain R.K., Master's Thesis, Memorial University of Newfoundland, (1979).

52 Souers P.C., Cryogenic Hydrogen Data Pertinent to Magnetic Fusion Energy, Lawrence Livermore Laboratory, University of California, Livermore, (1979).

53 Wooley H.W., Scott R.B., and Brickwedde F.G., J. Res. Natl. Bur. Stand. 41, 379 (1948).

54 Rudenko N.S., and Slyusar V.P., Zh. Fiz. Khim., 42, 242, (1968). The English translation: Russ. J. Phys. Chem., 42, 126, (1968).

55 Rudenko N.S., and Slyusar V.P., Zh. Fiz. Khim. 43, 781 (1969). The English translation: Russ. J. Phys. Chem., 43, 434 (1969).

56 May A.D., Varghese G., Stryland J.C., and Welsh H.L., Can. J. Phys. 42, 1058, (1964).

57 May A.D., and Poll J.D., Can. J. Phys. 43, 1836, (1965).

58 Gray C.G., and Van Krandendonk J., Can. J. Phys. 44, 2411, (1966).

59 Andibert M.M., Joffrin C., and Ducuing, Chem. Phys. Lett., 25, 158, (1974).

60 Wertheimer R.K., Molec. Phys., 35, 257, (1978).

61 Chang R.F., Burstyn H., and Sengers J.V., Phys. Rev. 19A, 866, (1979).

62 Jansoone V., Gielen H., Deboelpaep J., and Verbaue O.B., Physica 46, 213, (1970).

63 Balzarini D., and Wilcox L.R. , A.P.S., Spring Meeting Washington D.C., April, 1968.

64 Le Guillou J.C., and Zinn-Justin J., Phys. Rev. Lett., 39, 95, (1977).

65 Swinney H.L., and Cummins H.Z., Phys. Rev. 171, 152, (1968).

66 Kawasaki K., Ann. Phys. 61, 1, (1970).